OBSERVABILITY PROPERTIES OF RELATIVE STATE ESTIMATION BETWEEN TWO VEHICLES IN A GPS-DENIED ENVIRONMENT

By

ASAD N. AWAN

Bachelor of Science in Electrical Engineering,

University of Engineering and Technology,

Lahore, Punjab, Pakistan.

2011

Submitted to the Faculty of the
Graduate College of
Oklahoma State University
in partial fulfillment of
the requirements for
the Degree of
MASTER OF SCIENCE
May 12, 2017

OBSERVABILITY PROPERTIES OF RELATIVE STATE ESTIMATION BETWEEN TWO VEHICLES IN A GPS-DENIED ENVIRONMENT

Thesis Approved:

Dr. Weihua Sheng

Thesis Adviser

Dr. He Bai

Thesis Co-Adviser

Dr. Keith Teague

Committee Member

Dr. Sheryl Tucker

Dean of the Graduate College

Name: Asad N. Awan

Date of Degree: May 12, 2017

Title of Study: OBSERVABILITY PROPERTIES OF RELATIVE STATE ESTIMATION BETWEEN TWO VEHICLES IN A GPS-DENIED ENVIRONMENT

Major Field: Electrical Engineering

Abstract: One of the practical problems encountered in the coordination and cooperation of multi-UAS systems is to obtain the position and the orientation information of the neighboring vehicles while working in a GPS-denied environment. The research work is based on estimating the relative states between multiple vehicles and analyzing their observability properties. It has been divided into two sub-problems. First, the relative heading estimation between two unmanned aerial systems in the presence of constant disturbances is considered in a GPS-denied environment. Second, the observability properties of relative state estimation between two vehicles in bearing-only scenarios is investigated.

In the first problem, the nonlinear observability rank condition is employed and observability conditions of the relative states are established when the relative position between the two UAS is measured. In the first scenario, it is shown that if a UAS (say UAS 2) measures the position of another UAS (say UAS 1), the relative states between the two UAS, including the relative heading and the relative wind, and the airspeed and the heading rate of UAS 1, are locally weakly observable. The observability result holds even when UAS 2 is stationary. In the second scenario, observability properties of the relative states when UAS 1 is tracking a ground target using a feedback control are investigated. It is proved that the relative states and the range between UAS 1 and the target are locally weakly observable. The observability of the target range implies that UAS 2 can estimate the target position without observing the target.

In the second problem, global observability of the relative state estimation problem in bearing-only scenarios is investigated. It is assumed that one vehicle is equipped with a monocular camera sensor to obtain bearing measurements of the other vehicle. Global observability properties are investigated when the linear speeds and the angular velocities of both vehicles are constant. Unobservable scenarios when both vehicles are cruising or orbiting are also illustrated. It is further proved that the relative state is observable without communication between the vehicles. When both vehicles are orbiting, conditions on the angular velocities of the vehicles are developed to ensure observability.

Contents

List of Figures

List of Tables

Chapter 1

INTRODUCTION

1.1 Unmanned Aerial System

Unmanned Aerial system (UAS) refers to the aerial vehicles which operate without a human pilot. They are basically classified into three types i.e., unmanned aerial vehicles (UAVs), remotely piloted vehicles (RPVs) and drones. The terms UAV and RPV are used interchangeably, but an RPV is controlled or steered from a remote location and is always a UAV. However, a UAV may perform its operations autonomously or through preprogrammed navigation system, it need not always be an RPV. The term drone is used for aircraft controlled by radio signals and commonly referred to an aircraft with limited capabilities [13].

A typical UAS consists of air vehicles, ground control stations, payload and data links. Some UAS may include launch and recovery subsystems. They are now equipped with autopilots and human controllers which uses various navigation systems for preprogrammed missions. The accuracy of their flight and target identification is made capable by the use of different types of sensors. A few of them are described below:

1.1.1 Sensors

Main sensors used by UAS are as follows [32]:

Proprioceptive sensors are also called self-monitoring sensors. They are designed to monitor their self-maintenance and control their internal states. One of the commonly used proprioceptive sensors is an Inertial measurement unit (IMU) that is used to measure angular rate or the magnetic field around an object by using a combination of accelerometers and gyroscopes. The other common use of proprioceptive sensors is battery percentage monitoring, internal heat monitoring, and voltage and current sensing.

Degree of freedom (DOF) refers to both the amount and quality of sensors on-board.

- 6 DOF stands for 3-axis gyroscopes and accelerometers (a typical inertial measurement unit)
- 9 DOF refers to an IMU plus a compass
- 10 DOF refers to an IMU, compass and adds a barometer
- 11 DOF usually combine a GPS receiver to a 10 DOF system

Exteroceptive sensors are used to estimate an objects relative measurements with respect to another objects frame of reference. They are used to determine if an object/ robot is near another object and help them avoid collision. They can also be used to determine the distance of one object to another.The main types of exteroceptive sensors are listed below:

Contact Sensors are the sensors that send an object detection signal to the processor when a physical contact is established. They are mechanical switches that are used to detect a contact or the mechanical interactive forces and torques objects parts meet each other.

Range Sensors are used to measure the distance to objects in the area of their range. They are used for robot navigation and obstacle avoidance, or to recover the 3rd dimension for monocular vision. They work on one of the two principles: time-of-flight and triangulation.

Vision Sensors involves extraction and characterization of the information from images and to interpret the data to identify objects in the surrounding environment.

The common examples of exteroceptive sensors are Camera (CMOS, infrared), range sensors (radar, sonar, lidar).

1.1.2 Challenges in position estimation using GPS

The Global Positioning System, commonly abbreviated as GPS is a constellation of 24 well-spaced satellites-based navigation system orbiting the Earth to provide geographic locations to anyone who has a ground receiver. The accuracy of the GPS location estimate is from 10 to 100 meters. It is available for general use around the world. Briefly, here is how it works: [15]

21 GPS satellites are in orbit at around 10600 miles above the Earth. Three spare satellites are also launched in the space for emergency purposes, making it a system of 24 satellites. They are spaced in a way that 4 satellites will be above the horizon when viewed from any point of the Earth. They are equipped with a computer, a radio and an atomic clock. The clock and an estimate of its own orbit, the satellites continually broadcast their changing positions and time. The GPS receiver at the ground triangulated its own position by getting bearings from 3 out of 4 satellites. The final geographic location is shown in the form of longitudes and latitudes.

The main problem in estimating the position of moving body using a GPS is that there are different factors that degrade the GPS signal and affect the position accuracy as listed below [11]:

Signal multipath is an error that is caused by an increase in time travel of the GPS signal after it reflects off from an object like a building before it reaches the receiver which affects the accuracy. Similarly, a GPS satellite atomic clock is more accurate than the receiver's built-in clock so it may have very slight timing errors. Though, three satellites are enough for position measurement, but the more satellites available, the

Table 1.1: Classification of UAS [21]

Description	Weight (kg)	Range (m)	Endurance (h)	Airspeed (Knots)	Models
Small/Micro	≤ 5	10	≤ 5	≤ 100	Dragon Eye
Medium/ Light	5-50	≤ 100	$\leq 5-24$	≤ 250	RPO Midget
Larger/ Medium	50-200	100-400	$\leq 5-24$	≤ 250	Raven
Larger/ Heavy	5-2000	$\leq$ 400-15000	$\leq 5-24$	Any air Speed	A-160
Largest/ Super Heavy	≥ 2000	≥ 15000	≥ 24	Any air Speed	Global Hawk

more accuracy is achieved. This is also one of the reasons why GPS does not work good in underwater, indoors or underground. Moreover, accurate measurements are achieved when satellites are positioned at wide angles relative to one another whereas the accuracy in position is degraded when they are located in a line or in a tight grouping. Secondly, the reliability of position estimation on GPS is greatly halted as GPS signals are also prone to other unusual situations as listed below:

- Intentional Jamming
- Unintentional Interference
- Blockage in cluttered urban environment

Considering the problems in position estimation through the GPS navigation system, a lot of recent research is being conducted in developing GPS denied technologies. Through the GPS-denied environment, through the use of multiple sensors and by utilizing computer vision technology, the over-dependency on GPS has been reduced.

1.1.3 Classification of UAS

UAS has been classified into different categories according to the following parameters:

- By weight
- By range and endurance
- By altitude
- By wing loading
- By engine type

1.1.4 Applications of UAS

UAS has been used in different remote sensing applications due to their rapid response and cost effectiveness. They are used to perform multiple military and civil tasks where a mission/ observation is to carried out in a harmful environment. The adoption of remote sensing in archaeology and vegetation monitoring using UAS has become popular in the recent times [12]. Rapid response imaging using UASs has received attention as this has been demonstrated for road accident simulations and in many cases of forest fire monitoring. UAVs have also been proposed as platforms to monitor volcanoes. A final example of the flexibility of UAVs is their use in traffic monitoring [26].

1.2 Multi-UAS Systems

Autonomous flying vehicles or UASs have continuously been exploited in different commercial and civil as well as military applications for reconnaissance, explorations and detection, monitoring and disaster management. For many applications, a group of coordinated UASs can play a more important role than a single UAS. Multi-UAS systems can monitor a certain area much quickly or gather more information from different perspectives at the same time. To take benefit from this emerging technology, profound amount of research work is being done in field of Multi-UASs. The group of UASs working together can overcome the shortcomings of single UAS system. In this way, they can accomplish something better than the single unit. Multi-UASs exchange their sensor information, coordinate with one another to track and monitor targets, monitor activities and even collaborate to transport the payloads.

1.2.1 Classification of Multi-UAS Systems

The classification of Multi-UASs on the basis of coupling is as follows [8] :

Physical Coupling

UASs are physically connected to one another through some link and the motion of all UASs is dependent on others. The whole system is considered a single body when path planning is considered. It can only have small number of UASs, therefore, both centralized and distributed architectures can be used. One of the applications is to transport the payload from one position to another.

Formations

UASs are not linked physically but the movement of UASs is strictly controlled to maintain the formation. Path planning of the system can be considered as a single unit. For small number of vehicles, both centralized

and decentralized architecture can be used but for higher number of formations, decentralized technique is preferred.

Swarms

A group of vehicles whose interaction creates a collective behavior to accomplish a common goal. They are not physically linked or does not necessarily make formations. Usually large number of vehicles participate so scalability is a problem and a decentralized approach is advised.

Intentional Cooperation

UASs are programmed to follow specific trajectories to finish individual tasks which are part of a big task. No physical link, formations or any geometric configuration is expected between different UASs. Due to preservation of individuality of UASs, both centralized or decentralized architectures can be used.

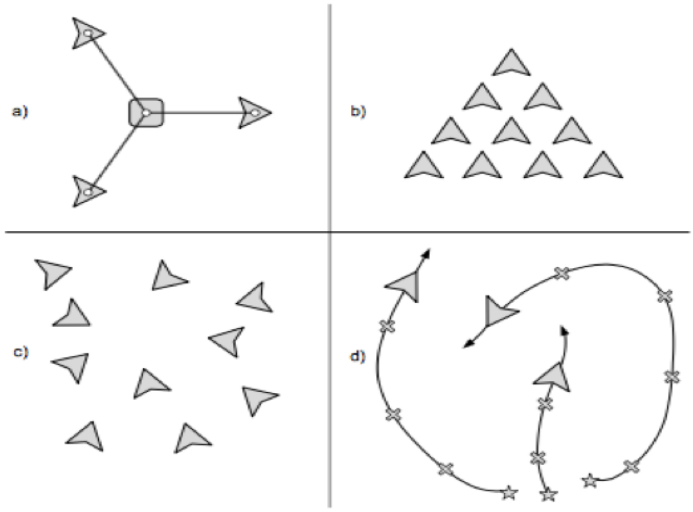

Figure 1.1: Classification of multiple UAS systems: a) Physical coupling, b) Formations, c) Swarms and d) Intentional cooperation [8]

1.2.2 Coordination and cooperation in Multi-UAS Systems

To accomplish different tasks, the coordination and cooperation of Multi-UASs plays a very critical part. Generally, the coordination refers to sharing the resources amongst the UASs, temporal and spatial. The former deals with syncing of multiple UASs whereas the later relies on space allocation amongst UASs. These concepts are used for UASs path planning in which the regular path planning concepts can be applied to multi-UAS scenario [20] [6]. The concept of cooperation revolves around a collective behaviour of UASs

to accomplish a common goal with some mechanized cooperation algorithms which results in a dramatic improvement in the total efficiency of the system [4]. The cooperation of multi-UAS system integrates the sensor information, control and path planning algorithms in an appropriated decisional architecture which is application dependent. The centralized architectures require more storage and computational capabilities but offers better cooperation amongst UASs whereas decentralized architecture offers better scalability. There are different benefits of using Mutli-UAS system as compared to a single UAS and are listed below [23]:

Multitasking

Multiple UASs collect information from different locations simultaneously to build models used to take decisions which can be time consuming for a single UAS.

Improved Efficiency

The total time for exploration and object detection using multi-UASs is drastically reduced as compared to single UAS, critically increasing the efficiency of the system.

Complementarities of Team Members

Multi-UAS system provides advantage over single UAS by exploiting their complementarities e.g., fixed wing aircrafts have better range and time of flight, whereas quadcopters are capable of having better manoeuvring abilities. They can work together and provide better results than working alone.

Redundancy

Multi-UAS system is more reliable as it is more fault tolerant and offer more flexibility incase of malfunction.

Cost Effective

A group of UASs performing tasks simultaneously is more cost effective and time saving as compared to a single UAS performing different tasks.

1.3 Target Handoff

A simple example of multi-UAS coordination is when UAS, tracking a target, can not continue its task and its job has to be handed over to a new UAS. This concept is known as target handoff. The need for target handoff arise from different reasons. In a practical scenario, a battery operated tracking UAS can have its battery level below certain values or a gasoline operated UAS needs refueling. There may be a scenario when

a more demanding target is to be located and the services of the current tracking UAS, with more tracking capabilities, are required. In these cases, one of the possibilities is to let go off the target due to the limitations of the current tracking UAS capabilities. The other and a much better approach is to handoff the target to a new UAS. The objective of target handoff is to enable another UAS to have a visual lock on the target and continue tracking.

One of the practical problems encountered in the coordination and cooperation of multi-UAS system is to get position and orientation information of the neighboring vehicle in a GPS-denied environment. However, it can obtained by estimating the relative position of the target as shown in Fig. 1.2. Suppose a UAS is tracking a moving object on ground or air. Let's call this a tracking UAS. The tracking UAS has a visual lock on the target. The other UAS being the handoff UAS. Let r_T represents the inertial position of target whereas r_t and r_h denotes the inertial position of tracking UAS and the handoff UAS respectively. Let R_{ab} show the rotation matrix between the frame a and frame b. Therefore, r_T^t represents the position of the target in the tracking UAS reference frame. If the handoff UAS can obtain an accurate estimate of $(r_T - r_h)^h$, the relative position of the target in the handoff frame, it can position its sensor to lock the target [3]

$$(r_T - r_h)^h = (r_t - r_h)^h + R_t^h (r_T - r_t)^t, \tag{1.1}$$

$$= (r_t - r_h)^h + R_h (R_t)^{-1} (r_T - r_t)^t, \tag{1.2}$$

To obtain promising results and a lock of target, the handoff UAS should obtain the following estimates: $(r_t - r_h)^h$, the relative position estimate of tracking and handoff UAS represented in the handoff frame $(r_T - r_t)^t$, the relative position between the tracking UAS and the target in the tracking reference frame $R_h(R_t)^{-1}$, the relative attitude between the two UASs. Here, it is assumed that $(r_T - r_t)^t$ is a known value by tracking UAS and handoff UAS can get it without any delay.

1.4 Summary of Thesis

The rest of the thesis is organized as follows. In chapter 2, literature of some important topics which are related to the main problems is reviewed. First, the concept of observability and lie derivative has been discussed. The study of different vehicle tracking methodologies has been done. One of the estimating techniques using Kalman filters has been discussed in detail. The concept of bearing only tracking has been reviewed. In the end, the problem of relative heading estimation between multi-vehicle in GPS denied environment has been analyzed. In the first part of the chapter 3, relative heading estimation between two Unmanned Aerial Systems is considered and observability properties of relative states between the two UASs in the presence of constant disturbances are examined. State observability properties are established when UAS 1 is tracking a stationary ground target using a feedback control. The simulation results demonstrate its

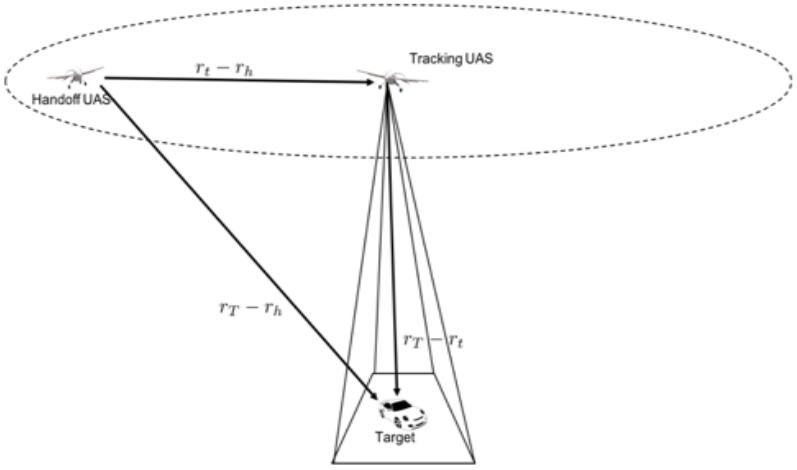

Figure 1.2: GPS denied Target Handoff problem [3]

effectiveness in estimating the relative states. In the second part of chapter 3, global observability properties are investigated while estimating the relative position and heading between two vehicles. Unobservable scenarios are illustrated and conditions on the angular velocities to ensure observability are also developed. In chapter 4, the experimental results have been shown. First, the detail of all the hardware used in the experiment has been provided. The software details and configuration of software is explained later. In the end, the experimental and simulation results have been shown. In chapter 5, conclusion and future work have been included.

Chapter 2

LITERATURE REVIEW

2.1 Observability and State Estimation

Observability analysis is a fundamental component of any real-time State Estimator. It is an estimate of the internal states of a system by the knowledge of its external outputs. Therefore, a system is observable if the current state is measured by only using the output sensors in a finite time period for any sequence of state and control vectors. It means that only by visualizing the output data of the system, the whole behaviour of the system can be determined. A state-space representation is a mathematical description of a physical system in the form of inputs, outputs and state variables where the state variables are on the axes and the vectors in that space represents the state of the system [18]. State estimation gives an estimate of internal states of a real physical system only from the input and output measurements. Practically, it is difficult to estimate the state of the system by just observing the inputs and outputs of the systems e.g., the exact information about the internal states of the cars inside the tunnel is difficult to know from someone viewing the cars exiting a tunnel from outside, though the velocities of the cars entering and exiting (input and output) is available. However, if the system is observable, the states of the system inside the tunnel can possibly be reconstructed only by its output measurements using the state estimator. It is similar to the scenario that when a car enters a tunnel, the GPS signal keeps on showing a moving car, even though, the GPS signal of the car has already been lost and no updated position of the car is received. It is through state estimators like Kalman filters etc that the next states are continually estimated even with a noisy sensor data or control commands with uncertain effects [1]

2.1.1 Review of Observability

For linear time-invariant (LTI) systems in the state space representation, there is a convenient test to check if a system is observable. Consider a single input single output (SISO) LTI system consists of n states [34]. The state equations are defined in terms of matrices A and B as shown in (2.1) whereas the output equations are expressed in terms of C and D matrices as shown in (2.2).

$$\dot{x} = Ax + Bu \tag{2.1}$$

$$y = Cx + Du \tag{2.2}$$

where the state vector x is a column vector of length n, the input vector u is a column vector of length r, A is an nxn square matrix of the constant coefficients a_{ij}, B is an nxr matrix of the coefficients b_{ij} that weight the inputs, y is a column vector of the output variables, C is an mxn matrix of the constant coefficients c_{ij} that weight the state variables, and D is an mxr matrix of the constant coefficients d_{ij} that weight the system inputs [34]. The matrices A and B are properties of the system and are determined by the system structure and elements. The output equation matrices C and D are determined by the particular choice of output variables. For the SISO LTI system defined in (2.1) - (2.2), if the row rank of the following observability matrix

$$O = \begin{bmatrix} C \\ CA \\ CA^2 \\ \vdots \\ CA^{(n-1)} \end{bmatrix} \tag{2.3}$$

is equal to n, then the system is observable. The rationale for this test is that if n rows are linearly independent, then each of the states is viewable through linear combinations of the output variables.

2.1.2 Nonlinear Observability

Lets consider a nonlinear system $\sum$ of the following form: [17]

$$\dot{x} = f(x,u), x \in M \subseteq R^n \tag{2.4}$$

$$y = h(x) \subseteq R^m \tag{2.5}$$

Please note that the two states x_0, $x_1 \in$ M are said to be indistinguishable, if for every admissible input $u(t)$, $t_0 \leq t \leq t_{end}$, identical output results:

$$y(t;x_0) = y(t;x_1) \quad for \quad t_0 \leq t \leq t_{end} \tag{2.6}$$

The nonlinear system $\sum$ is observable at x_0, if $I(x_0) = x_0$. The nonlinear system $\sum$ is observable, if $I(x) = x$ for all $x \in M$.

Notation: $I(x_0)$ = set of all points that are indistinguishable from x_0.

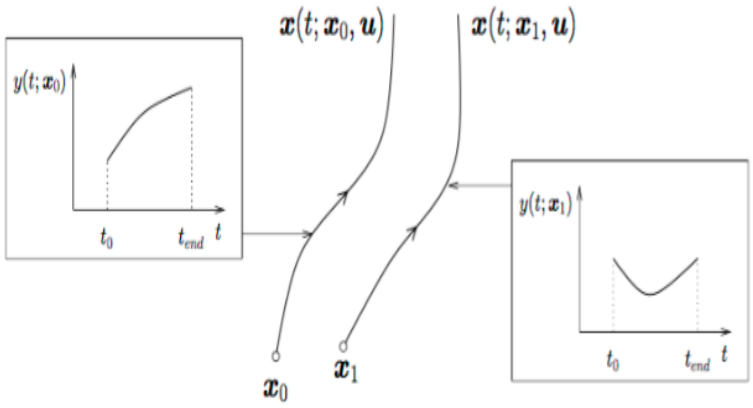

Figure 2.1: Nonlinear Observability [17]

It must be noted that the observability is sometimes called 'global observability'. The reconstruction of x from measurement data may be possible for certain inputs u(t), $t_0 \leq t \leq t_{end}$ only.

Local Observability

The nonlinear system $\sum$ is locally observable at x_0, if for every open neighbourhood N of x_0 and for every solution x(t) completely in N, $I_N(x_0) = x_0$. The nonlinear system $\sum$ is locally observable, if $I_N(x) = x$ for all $x \in M$.

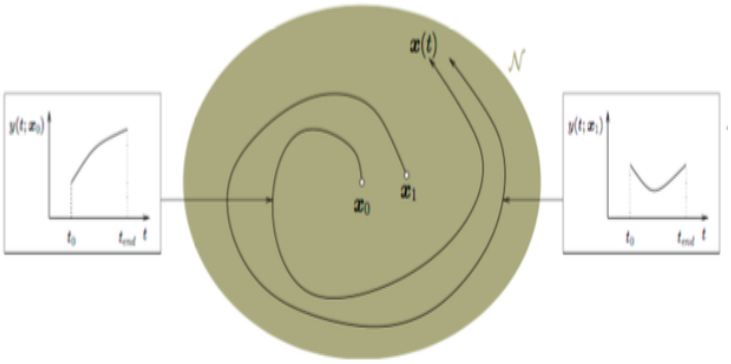

Figure 2.2: Local Observability [17]

Here, it must be noted that the local observability is a stronger property than observability.

Weak Observability

The nonlinear system $\sum$ is weakly observable at x_0, if there is some neighbourhood V of x_0 where $I(x_0) \bigcap V = x_0$. The nonlinear system $\sum$ is weakly observable, if such a neighbourhood V exists for all $x \in M$.

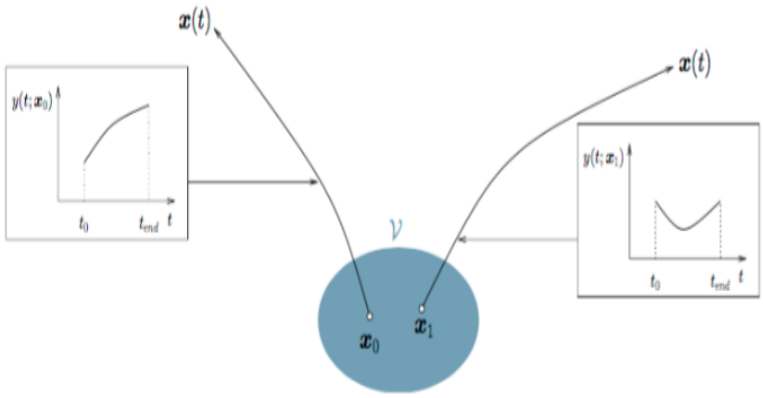

Figure 2.3: Weak Observability [17]

Locally Weak Observability

The nonlinear system $\sum$ is locally weakly observable at x_0, if there is some neighbourhood V of x_0 where $I(x_0) \bigcap V = x_0$, for all solutions x(t) completely in any neighbourhood N of x_0. System $\sum$ is locally weakly observable if this property holds for all $x \in M$. The nonlinear system $\sum$ is weakly observable, if such a neighbourhood V exists for all $x \in M$.

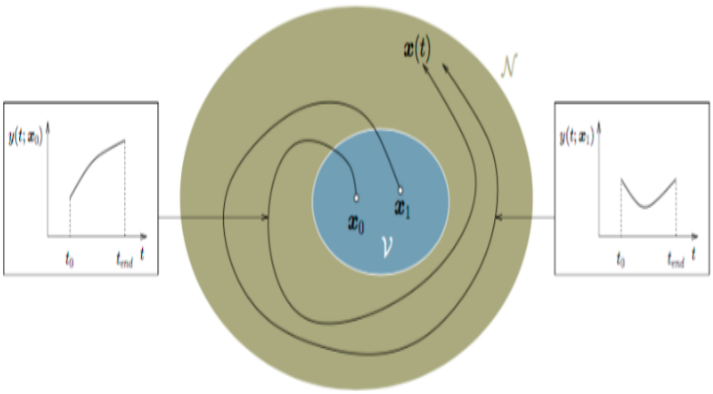

Figure 2.4: Locally Weak Observability [17]

Lie Derivative

Consider an autonomous system

$$\dot{x} = f(x) \tag{2.7}$$

$$y = h(x) \tag{2.8}$$

The derivative of the measurements:

$$\frac{dy}{dt} = \frac{\partial y}{\partial x}\frac{dx}{dt} = \frac{\partial h}{\partial x}f(x) \tag{2.9}$$

Higher derivative of y can be written compactly by introducing the operator $L_f[.]$ (Lie Derivative) [17] where $L_f[h] = \frac{\partial h}{\partial x}f(x)$ is the time derivative of h along the system trajectory x

$$\frac{d^2y}{dt^2} = \frac{\partial y}{\partial x}\left(\frac{\partial y}{\partial x}f(x)\right)f(x) = L_f[L_f[h]] = L_f^2[h] \tag{2.10}$$

$$\frac{d^ky}{dt^k} = L^k[h] \tag{2.11}$$

The observability mapping $Q(x)$ for the autonomous system will be defined as:

$$\begin{pmatrix} y \\ \dot{y} \\ \ddot{y} \\ \vdots \end{pmatrix} = \begin{pmatrix} L_f^0[(x)] \\ L_f^1[(x)] \\ L_f^2[(x)] \\ \vdots \end{pmatrix} = Q(x) \tag{2.12}$$

$Q(x)$ defines a set of nonlinear equations for determining x from $y, \dot{y}, \ldots$ For a general nonlinear system, the number of time derivatives is not fixed which means that Cayley Hamilton theorem is not applicable. For LTI system, $Q(x) = O(x)$ with Kalman observability matrix O.

The nonlinear system $\sum$ satisfies the observability rank condition at x_0, if $\frac{\partial Q(x)}{\partial x}$ at x_0 contain n-linearly independent row vectors. The observability indices of a given system are not unique. The observability rank condition is sufficient but not necessary for locally weak observability [17]

2.2 Kalman Filter

Kalman Filter is a recursive data processing tool to measure predicted values through an iterative mathematical process. It uses a series of measurements and consecutive data inputs measured over time to quickly

estimate the unknown state variables e.g., position, velocity, heading of the object being measured which contains statistical noise, unpredicted errors and other uncertainties. It uses a feedback loop that begins with estimating the states from the previous states. The measured values from a sensor act as a feedback to the filter. The filter basically consists of time update and measurement update equations which estimates current state ahead of time and adjust the projected estimate by an actual measurement of that time, respectively [35].

Let say 50 consecutive data points are considered and a distribution of these values is made, and the average is taken which must be very close to the true value. But it requires lots of inputs to give a true estimate. However, Kalman filter uses very few data inputs to start giving values that are very close to the true estimate. There are numerous applications of Kalman Filter in technology which includes navigation and control of aircrafts etc. It is also used in the field of controls and robotics for path planning and trajectory optimization etc.

The main difference between Kalman and extended Kalman filter is that Kalman filter could not work with the Nonlinear systems whereas Extended Kalman filters can be used to solve nonlinear systems.

2.2.1 Example (Temperature measurement)

Lets consider a very simple example of measuring a temperature value from the thermometer. The thermometer is not very accurate and there is some uncertainty in the data measurements. As shown in Fig. 2.5, the x-axis shows the time on which continuous sample points have been taken at regular intervals. The y-axis shows the temperature. The little crosses are the measured values at regular intervals. It will take a lot of time to average these values to get an estimate of the real temperature because of lots of variation in the data measured. However, the Kalman filter predicts the actual temperature much faster and accurately.

It starts with taking an initial estimate and it does not matter what the initial estimate is. In the initial estimate, a certain amount of uncertainty or error is considered. As data points start coming in and an iterative process begins, the Kalman filter starts estimating the values. It does not take too many inputs to reach close to the actual temperature value.

2.2.2 Flowchart of a simple measured value

The process of implementing Kalman filter consists of basic three basic equations or calculations which always go on iteratively. The first is calculating the Kalman gain. Next, the current estimate is evaluated and it is updated on regular intervals and, finally, the new error/uncertainty in estimate is calculated [33].

1. Calculate the Kalman Gain

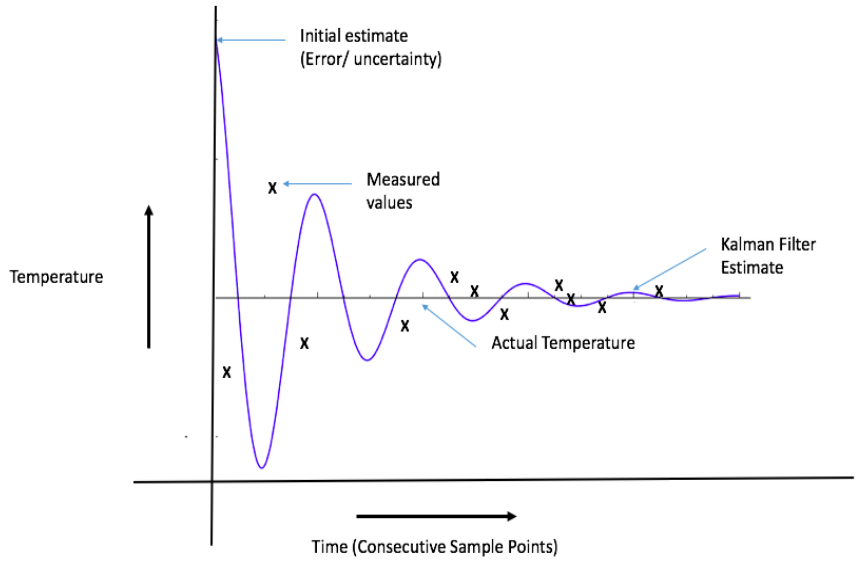

Figure 2.5: Temperature measurement

2. Calculate the current estimate

3. Calculate new error in estimate

The first step is to calculate the Kalman gain or gain, the error in the estimate needs to be known which is either the previous error in estimate or the original error. Each time the error is estimated (step-3 in Kalman Filtering), the error estimate is updated and fed to measure the new Kalman gain. The other parameter required to calculate the gain is the error in data input. Both of these feed into the calculations and come up with a new gain. The gain gives a relative importance between the error in the estimate versus the error in the data input. If the error in the estimate is smaller, more importance is put in it and if the error in the input is smaller, more importance is put in it. Kalman Gain = KG

Error in estimate = E_{EST}

Error in measurement = E_{MEA}

$$KG = \frac{E_{EST}}{E_{EST} + E_{MEA}}, 0 \leq KG \leq 1 \tag{2.13}$$

Secondly, the Kalman gain is fed into the calculations of current estimation. New estimate depends on the gain. Beside gain, it also depends on the previous estimate or the original estimate. The other required data will be the data input. The gain will decide how much to put on the previous estimate and the new measured value.

In the last step, for the calculation of new error estimate, the gain and the current estimate are needed. It is

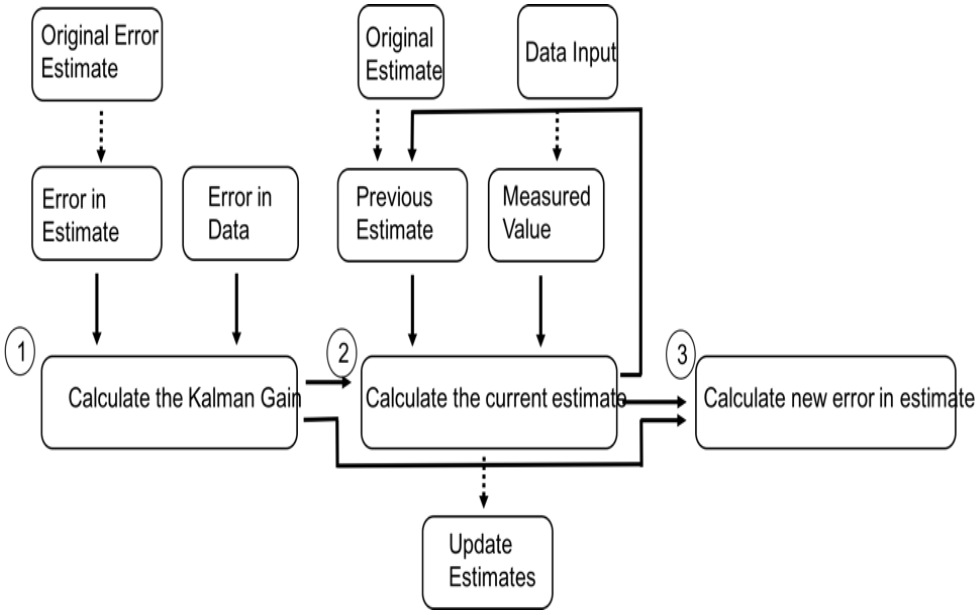

Figure 2.6: Flowchart for Kalman Filter Estimation

then fed to calculate the new gain in the next iterative cycle and process continues to refine and gets closer to the true value.

Current estimate = EST_t

Error in current estimate = $E_{EST}(t)$

Previous Estimate = EST_{t-1}

Measurement = MEA

$$EST_t = EST_{t-1} + KG(MEA – EST_{t-1}) \tag{2.14}$$

$$E_{EST(t)} = \frac{(E_{MEA})(E_{EST(t-1)})}{(E_{MEA}) + (E_{EST(t-1)})} = [1 - KG](E_{EST(t-1)}) \tag{2.15}$$

The earlier discussion was regarding a single parameter based system. However, the real applications of Kalman filtering is performed on a set of parameters representing a dynamic system. Before starting, lets define a few terms:

1. The mathematical model of the system, represented by matrices A, B, and H.
2. An initial estimate about the complete state of the system, given as a vector x.
3. An initial estimate about the error of the system, given as a matrix P.
4. Estimates about the general process and measurement error of the system, represented by matrices Q and R respectively.

During each time step, you are expected to give it the following information:

- A vector containing the most current control state (vector ”u”). This is the system’s guess as to what it did to affect the situation (such as steering commands).
- A vector containing the most current measurements that can be used to calculate the state (vector ”z”).

After the calculations, you get the following information:

- The most current estimate of the true state of the system.
- The most current estimate of the overall error of the system.

Kalman Filter equations are given below:

State Prediction (predicts the new state)

$X_{Predicted} = AX_{n-1} + BU_n$

Covariance Prediction (Predicts the error)

$P_{Predicted} = AP_{n-1}A^T + Q$

Innovation (Compares measured values against estimated)

$Y = Z_n – HX_{Predicted}$

Innovation Covariance (Compares real error against estimated)

$S = HP_{Predicted}H^T + R$

Kalman Gain (Moderates the prediction)

$K = P_{Predicted}H^T S^{-1}$

State update (New estimate of state)

$X_n = X_{Predicted} + Ky$

Covariance update (New estimate of error)

$P_n = (I - KH)P_{Predicted}$

Inputs

U_n = Control vector. This indicates the magnitude of any control system’s or user’s control on the situation.

Z_n = Measurement vector. This contains the real-world measurement in this time step.

Outputs

X_n = Newest estimate of the current ”true” state.

P_n = Newest estimate of the average error for each part of the state.

Constants

A = State transition matrix. Basically, multiply state by this and add control factors, and you get a prediction of the state for the next time step.

B = Control matrix. This is used to define linear equations for any control factors.

H = Observation matrix. Multiply a state vector by H to translate it to a measurement vector.

Q = Estimated process error covariance. Finding precise values for Q and R are beyond the scope of this guide.

R = Estimated measurement error covariance. Finding precise values for Q and R are beyond the scope of this guide.

2.3 Bearing Only Tracking

Bearing-only tracking is a method to estimate the position and target of the vehicle by only using the angular measurements or bearing angles. Bearing angle is the angle between the horizontal plane of the observer i.e., sensor, and the line of sight between the target and the observer. The sensor which can be a monocular camera provides the bearing angle measurements. One of the two main issues that make the process of tracking hard is the high degree of nonlinearity of the measurement process. The second one being the target not fully observable if the tracking vehicle or sensor platform does not out maneuver the target [24] . Incase, correct maneuver is not done, sufficient information is not avilable to estimate the range of the target. The other practical problem is the estimation of vehicle trajectory from a noise corrupted sensor measurements.

Fig. 2.7 shows an example of bearing-only tracking problem and the importance of tracking vehicle maneuvering. It is considered that the target vehicle has a constant velocity and it is currently not maneuvering. The vector from point D-E' shows the target motion. The motion of the observer or tracking vehicle is shown from point A-B and then from point B-C. If only the observer constant motion from point point A-B and target motion from point D-E is considered, the tracking algorithm can not estimate the target's trajectory or range as several target trajectories can generate the same bearing angles. The maneuvering of observer (two distinct legs) is necessary as shown from A-C in Fig. 2.7 to estimate the target's trajectory and allows to have a unique solution. Multiple maneuvering legs are required to get a satisfactory estimation. This example only considers a constant motion of observer and target . The complexity of the estimation problem increases when the measurement noise and environmental disturbances are considered, and the target maneuvers.

Different estimation algorithms have been proposed to the bearing-only problem which have varying outcomes. Extended Kalman filter (EKF)is one of the common methods when dealing with nonlinear models. EKF often yields good estimates and accurate covariance estimates, it is known to have diverged if the degree

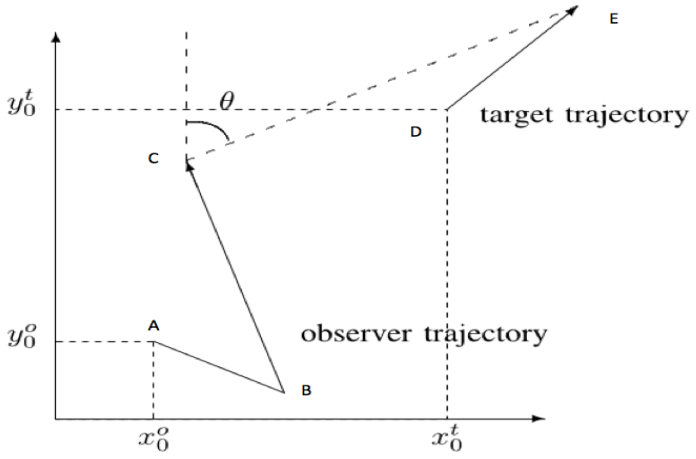

Figure 2.7: Bearing-only target-observer encounter [24]

on nonlinearity is high or the filter is not properly initialized. The polar coordinate system representation for the target motion is used to overcome the initialization issue based on bearing information. However, it is assumed that the target has a straight trajectory and bearing measurements are noisefree to the maximum extent possible. Under these assumptions, this method can calculate target velocity components from three consecutive bearing. With the availability of fourth bearing, this method can calculate the range to target with good accuracy. For noisy measurements, the initialization is done through a batch of measured bearings. Another method used to estimate the trajectory of vehicles using bearing only measurements is the modified polar coordinate filter which considers bearing, bearing and range rate, and reciprocal range as state variables. It isolates the propagation of observable states in the covariance matrix during the first leg. It results in a normalized solution in the first leg and the remaining states converging on the following legs.

2.4 Relative Heading Estimation in GPS-Denied Environments

The paper [3] proposes a solution for estimating relative heading between two fixed wing aircrafts to achieve target handoff in a GPS denied environment. The results are achieved by estimating the relative pose between the aircrafts. It is assumed in the paper that the Unmanned Aerial System (UAS) has been equipped with inertial Navigation System (INS), which measures the pitch and roll angles. In this way, the 6 DOF system has been reduced to just relative heading estimation i.e., yaw estimation, considering that the tracking UAS can transmit the pitch and roll angles to the handoff UAS. It is considered that the relative position is measured by the handoff UAS. Under these assumptions, the paper examined the relative states between the UAS to achieve the target handoff when the only measurement available is the relative position between the UAS. It is shown that the relative heading is locally weakly observable when relative position is measured.

2.4.1 Relative Heading Estimation

The paper defines tracking UAS as UAS 1 and the handoff UAS as UAS 2. It is assumed that both the UAS are flying at the same altitude. The kinematics of the system is given by:

$$\dot{p}_i = v_i \begin{bmatrix} \cos\theta_i \\ \sin\theta_i \end{bmatrix} \tag{2.16}$$

$$= v_i \begin{bmatrix} \cos\theta_i \\ \sin\theta_i \end{bmatrix} \tag{2.17}$$

$$\dot{\theta}_i = \omega_i \tag{2.18}$$

where $p_i \in \Re^2$ and θ_i is the heading of UAS i in the inertial frame. v_i and ω_i are the linear and angular speeds, respectively.

Here, the speeds ω_1 and v_1 are considered constant which means that the UAS-1 is either cruising with a constant velocity or in an orbit. Secondly, it is assumed that UAS-2 has ω_2 and v_2 information which means that the UAS-2 is equipped with an airspeed sensor that measures v_2 and an INS that estimates the roll angle ϕ_2.

The relative position in UAS-2 frame is defined as

$$\widetilde{p_2} = R_{\theta_2}^T \widetilde{p} \tag{2.19}$$

$$\tag{2.20}$$

where R_{θ_i} is defined as the attitude of the ith UAS, also known as the *Yaw* and is represented by

$$R_{\theta_i} = \begin{bmatrix} \cos\theta_i & -\sin\theta_i \\ \sin\theta_i & \cos\theta_i \end{bmatrix} \tag{2.21}$$

$$\tag{2.22}$$

The observability of the relative heading and position in UAS 2's frame is analyzed when the relative position between the two UAS is available. The relative position in UAS 2 frame is defined as

$\widetilde{p_2} = R_{\theta_2}^T (p_1 - p_2)$, the relative heading is defined as $\tilde{\theta} = \theta_1 - \theta_2$, and the state vector x as $x = [\widetilde{p_2}^T, \widetilde{\theta}, \omega_1, v_1] \in \Re^5$.

The system dynamics is represented by the following equation

$$\dot{x} = f(x) = \begin{bmatrix} \omega_2 x_2 + C_{x_3} x_5 - v_2 + x_6 \\ -\omega_2 x_1 + S_{x_3} x_5 + x_7 \\ x_4 - \omega_2 \\ 0 \\ 0 \end{bmatrix} = \begin{bmatrix} \dot{\widetilde{P_{2_1}}} \\ \dot{\widetilde{P_{2_2}}} \\ \dot{\theta} \\ \dot{\omega_1} \\ \dot{v_1} \end{bmatrix} \tag{2.23}$$

It is assumed that UAS-2 can measure $\widetilde{p_2}$, The relative position of UAS 1 in UAS 2's frame is given by $\widetilde{p_2}$ and the measurement equation is

$$y = \widetilde{p_2} = \begin{bmatrix} x_1 & x_2 \end{bmatrix}^T = Hx \tag{2.24}$$

where

$$H = \begin{pmatrix} 1 & 0 & 0 & 0 & 0 & 0 & 0 \\ 0 & 1 & 0 & 0 & 0 & 0 & 0 \end{pmatrix} \tag{2.25}$$

The nonlinear observability rank condition is used to determine if the system is locally weakly observable. Specifically, the matrix ℓ_k is calculated which is given by

$$\ell_k = \begin{bmatrix} L^0_{fy} \\ L^1_{fy} \\ \vdots \\ L^k_{fy} \end{bmatrix} \tag{2.26}$$

where $L^0_{fy} = y$ and $L^i_f y = \frac{\partial}{\partial x}[L^{i-1}_f y] f(x)$

If the matrix $\frac{\ell_k}{\partial x}$ is a full rank matrix i.e., 5 in this case, then the state vector x is locally weakly observable. The following proof shows that the state vector x is locally weakly observable when $x_5 = v_1 \neq 0$.

L^1_{fy} is calculated and shown below as

$$L^1_{fy} = \begin{bmatrix} \omega_2 x_2 + C_{x_3} x_5 - v_2 \\ -\omega_2 x_1 + S_{x_3} x_5 \end{bmatrix} \tag{2.27}$$

which leads to

$$\frac{\partial \ell_1}{\partial x} = \begin{bmatrix} 1 & 0 & 0 & 0 & 0 \\ 0 & 1 & 0 & 0 & 0 \\ 0 & \omega_2 & -S_{x_3} x_5 & 0 & C_{x_3} \\ -\omega_2 & 0 & C_{x_3} x_5 & 0 & S_{x_3} \end{bmatrix} \tag{2.28}$$

It is of rank 4 matrix if x_5 is non-zero.

Next, L^2_{fy} is calculated

$$L^2_{fy} = \frac{\partial L^1_{fy}}{\partial x} f(x)$$

$$= \begin{bmatrix} \omega_2(-\omega_2 x_1 + x_5 S_{x_3}) - x_5 S x_3(x_4 - \omega_2) \\ -\omega_2(\omega_2 x_2 + x_5 C_{x_3} - v_2) + x_5 C_{x3}(x_4 - \omega_2) \end{bmatrix}$$

$$= \begin{bmatrix} -\omega_2^2 x_1 + x_5 S_{x_3}(2\omega_2 - x_4) \\ -\omega_2^2 x_2 - x_5 C_{x_3}(2\omega_2 - x_4) + \omega_2 v_2 \end{bmatrix} \tag{2.29}$$

where

$$\frac{\partial L^2_{fy}}{\partial x} = \begin{bmatrix} -\omega_2^2 & 0 & x_5 C_{x_3}(2\omega_2 - x_4) & -x_5 S_{x_3} & S_{x_3}(2\omega_2 - x_4) \\ 0 & -\omega_2^2 & x_5 S_{x_3}(2\omega_2 - x_4) & x_5 C_{x_3} & -C_{x_3}(2\omega_2 - x_4) \end{bmatrix} \tag{2.30}$$

$$\frac{\partial \ell_2}{\partial x} = \begin{bmatrix} 1 & 0 & 0 & 0 & 0 \\ 0 & 1 & 0 & 0 & 0 \\ 0 & \omega_2 & -S_{x_3} x_5 & 0 & C_{x_3} \\ -\omega_2 & 0 & C_{x_3} x_5 & 0 & S_{x_3} \\ -\omega_2^2 & 0 & x_5 C_{x_3}(2\omega_2 - x_4) & -x_5 S_{x_3} & S_{x_3}(2\omega_2 - x_4) \\ 0 & -\omega_2^2 & x_5 S_{x_3}(2\omega_2 - x_4) & x_5 C_{x_3} & -C_{x_3}(2\omega_2 - x_4) \end{bmatrix} \tag{2.31}$$

It is a rank 5 matrix if x_5 is non-zero which proves that x is locally weakly observable.

It is concluded from the above statement that when the state vector x is locally weakly observable, all the states of x can be estimated with accuracy. It indicates that the relative heading between the two UAS can also be estimated when the relative position measurements are available. It also shows that the linear and angular velocity of UAS 1 can also be estimated. It means that UAS 1 does not need to communicate its velocities to UAS 2 and relative heading can still be achieved. It leads to communication savings. An interesting observation is that the linear and angular velocities of UAS 2 can be zero which means that UAS 2 can be stationary i.e., an observatory point.

2.4.2 Simulation Output

In Fig. 2.8, the simulation output of estimated results of the system defined in kinematics (2.18) with the measurements shown in (2.24). The extended kalman filter is used to track the a circular vehicle moving with linear velocity of 13m/s and an angular velocity of 0.3rad/s. The true value of the position of the vehicle is

shown in red in the top left figure. Our EKF estimate of the position of the vehicle is accurate and shows the circular motion of the vehicle. It is to be noted that, though, EKF results are accurate in this case, it is not always the case. The initialization of EKF is a big challenge and the estimated results may not converge with the true values if proper initialization of EKF filter in not done. In this simulation, it has been shown that all the states in the state vector x can be estimated which proves the the state vector x is observable.

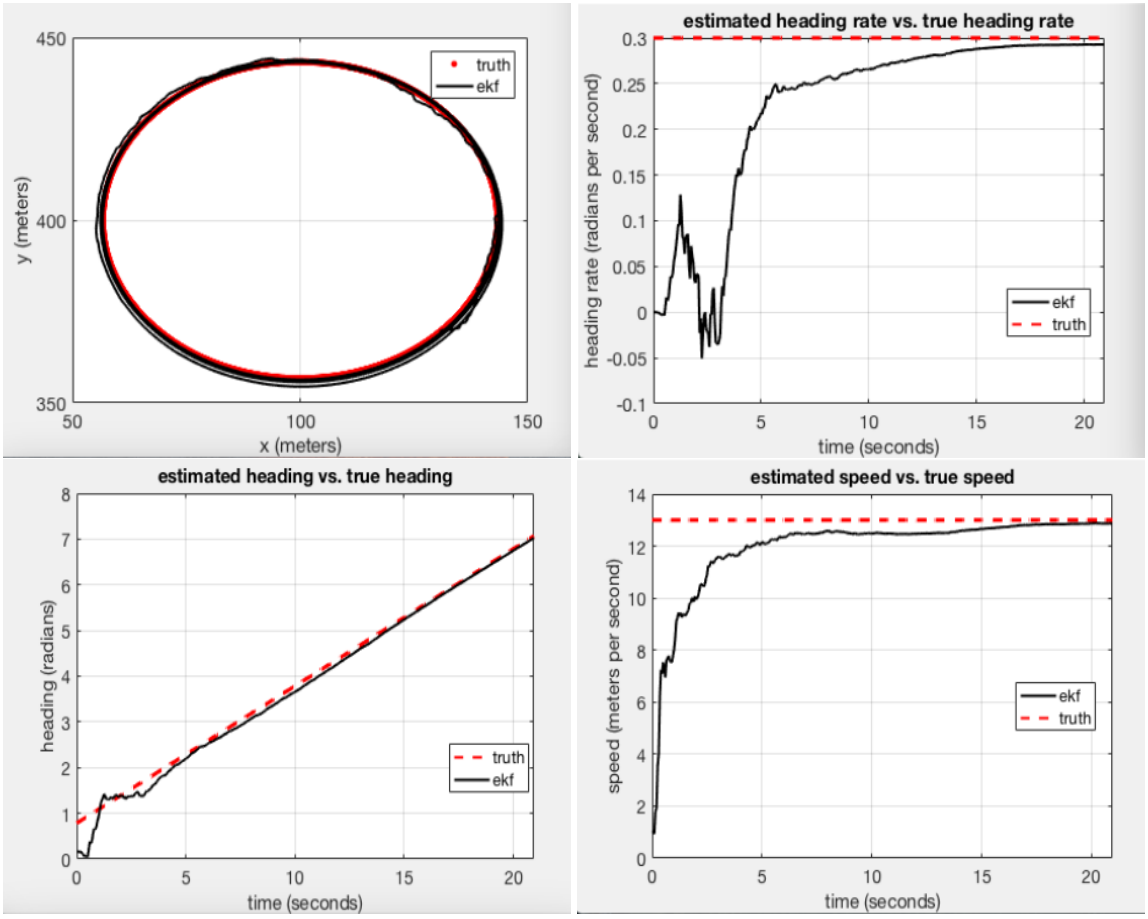

Figure 2.8: Simulation output of Extended Kalman Filter. Top left figures shows EKF tracking an object moving in a circle. Top right, Bottom left and Bottom right figures show the estimated results of heading rate, heading and speed as compared to true heading rate, heading and speed, respectively.

Chapter 3

OBSERVABILITY PROPERTIES OF RELATIVE STATE ESTIMATION

In the first section of this chapter, relative heading estimation between two Unmanned Aerial Systems (UAS) is considered. Observability properties of relative states between the two UAS in the presence of constant disturbances are examined. It is assumed that UAS 2 measures UAS 1's position in its own frame. First, observability conditions of the relative states when UAS 1 maintains a constant heading rate and a constant airspeed under the disturbance are presented. Next, state observability properties when UAS 1 is tracking a stationary ground target using a feedback control is established. In this case, the heading rate is non-constant. An extended Kalman filter (EKF) is designed and simulations to demonstrate its effectiveness in estimating the relative states are conducted.

In the second section, global observability properties of relative state estimation in bearing-only scenario are investigated when the linear speeds and the angular velocities of both vehicles are constant. Observability conditions when the velocity information of vehicle 1 is communicated to vehicle 2 are established. Unobservable scenarios when both vehicles are cruising or orbiting are illustrated. It is further proved that the relative state is observable without communication between the vehicles, if vehicle 1 and 2 are orbiting and cruising, respectively. When both vehicles are orbiting, conditions on the angular velocities of the vehicles to ensure observability are developed.

3.1 Relative Heading Estimation under Constant Disturbances

In [3], the authors consider a target handoff problem between two UAS in GPS-denied environments. To ensure handing off the target tracking responsibility from UAS 1 to UAS 2, UAS 2 needs to estimate the relative states between the two UAS, including the relative position and the relative heading. Reference [3] shows that if the relative position is measured, the relative heading is observable for UAS 2 even if UAS 1 does not communicate its airspeed and heading rate information. In [16], the authors present a navigation algorithm for relative pose estimation in GPS-denied environments. The algorithm uses inertial sensors and computer vision techniques to estimate the relative states between two UAS. Reference [14] and [31] outline different filter techniques to estimate the relative pose between two UAS. These techniques can be used in cooperative missions, such as formation flight and aerial refueling.

The previous work [3] is extended and relative heading estimation under constant disturbances is considered, such as a constant wind field. To address the estimation problem, the nonlinear observability rank condition in [17] is employed and observability conditions of the relative states are established when the relative position between the two UAS is measured. It is assumed that the vehicles do not exchange their linear and angular speeds, which is different from most of the existing work on relative localization, e.g., [10, 22, 28].

In the first scenario, UAS 1 maintains a constant heading rate and a constant airspeed in the presence of the constant disturbance. It is shown that if UAS 2 measures the position of UAS 1 and if the heading rate of UAS 1 is non-zero, the relative states between the two UAS, including the relative heading and the relative wind, and the airspeed and the heading rate of UAS 1, are locally weakly observable. The observability result holds even when UAS 2 is stationary.

In the second scenario, observability properties of the relative states when UAS 1 is tracking a ground target using a feedback control are investigated. Specifically, the tracking method developed in [27] to control the heading rate of UAS 1 are used. This tracking method ensures that the target remains in the field of view of a fixed angle camera on UAS 1 in the presence of the disturbance. The resulting heading rate is time-varying and the trajectory is elliptical. It is then proved that the relative states and the range between UAS 1 and the target are locally weakly observable. The observability of the target range implies that UAS 2 can estimate the target position without observing the target.

In [3], it is assumed that both UAS are at the same altitude and consider the following 2D kinematics of the two UAS [5]

$$\dot{p}_i = \begin{bmatrix} v_i c_{\psi_i} \\ v_i s_{\psi_i} \end{bmatrix} \tag{3.1}$$

$$\dot{\psi}_i = \omega_i = \frac{g}{v_i} \tan(\phi_i), \quad i = 1, 2, \tag{3.2}$$

where $p_i \in \mathbb{R}^2$ are the north-east positions of UAS i in the inertial frame, v_i and ω_i are the linear and angular speeds, respectively, and g is the gravitational constant.

In [3], the following assumptions are made:

Assumption 1: The speeds ω_1 and v_1 are constant. ■

Assumption 2: UAS 2 has ω_2 and v_2 information. ■

Assumption 1 implies that UAS 1 is either cruising with a constant velocity or in an orbit. Assumption 2 is satisfied when UAS 2 is equipped with an airspeed sensor that measures v_2 and an INS that estimates ϕ_2 in (3.2).

The relative position measured in UAS 2's frame as $\widetilde{p}_2 \in \mathbb{R}^2$ are defined, the relative heading as $\widetilde{\psi} = \psi_1 - \psi_2$,

and a state vector $x \in \mathbb{R}^5$ as

$$x = [\widetilde{p}_2^T, \widetilde{\psi}, v_1, \omega_1]^T. \tag{3.3}$$

Note that

$$\widetilde{p}_2 = R_{\psi_2}^T (p_1 - p_2), \tag{3.4}$$

where $R_{\psi_i} \in SO(2)$ is the attitude matrix of the ith UAS defined as

$$R_{\psi_i} = \begin{bmatrix} c_{\psi_i} & -s_{\psi_i} \\ s_{\psi_i} & c_{\psi_i} \end{bmatrix}. \tag{3.5}$$

The kinematics of x is given by

$$\dot{x} = \begin{pmatrix} \omega_2 x_2 + c_{x_3} x_4 \\ -\omega_2 x_1 + s_{x_3} x_4 \\ x_5 \\ 0 \\ 0 \end{pmatrix} + \begin{pmatrix} -v_2 \\ 0 \\ -\omega_2 \\ 0 \\ 0 \end{pmatrix}, \tag{3.6}$$

where x_i is the ith element of x.

Employing the observability rank condition in [17], the following result are proved in [3]:

Proposition 1: Consider the kinematics (3.60) with the relative position measurement $\widetilde{p}_2$, where x is defined in (3.3). Suppose that Assumption 1 and 2 hold. Then the state vector x is locally weakly observable if $x_4 = v_1 \neq 0$. ■

Proposition 1 requires that UAS 1 be moving for the observability of x. This is intuitive since the relative position measurement does not contain any information of the relative heading when UAS 1 is stationary. Proposition 1 also indicates that the unknown constants v_1 and ω_1 are observable and can be estimated. Thus, UAS 1 does not need to transmit those two states to UAS 2, leading to communication savings. In addition, Proposition 1 holds when v_2 and ω_2 are zero, which means that UAS 2 can be a stationary vehicle, e.g., a ground station.

Section 3.1.1 and 3.1.2 outline the observability conditions for relative heading estimation between two aircraft under constant disturbances such as wind. Our objective is to analyze whether the relative states between UAS 1 and UAS 2 are observable in the presence of the disturbances. In Section 3.1.1, an open-loop scenario is considered, where UAS 1 is not tracking a ground target. Due to the disturbance, the trajectory of UAS 1 is spiral. It is shown that state observability is ensured if UAS 2 measures the relative position to UAS 1 and if UAS 1 has a non-zero constant heading rate. In Section 3.1.2, a closed-loop scenario is considered, where UAS 1 counteracts the effect of the disturbance and tracks a stationary ground target. It is then proved that the relative states between the two UAS are observable given the relative position measurements. The

range to the target from UAS 1 is also observable. Section 3.1.3 presents a simulation example to demonstrate that the relative states can be estimated by an EKF.

3.1.1 Relative heading estimation without target tracking

Let the unknown constant disturbance affecting UAS i be $z_i \in \mathbb{R}^2$. Modify (3.1) and (3.2) and obtain the kinematics of UAS i under the disturbance z_i, $i = 1, 2$, as

$$\dot{p}_i = v_i \begin{bmatrix} c_{\psi_i} \\ s_{\psi_i} \end{bmatrix} + z_i, \tag{3.7}$$

$$\dot{\psi}_i = \omega_i = \frac{g}{v_i} \tan(\phi_i). \tag{3.8}$$

Note that (3.7) and (3.8) can also model ground vehicles. When $v_i = 0$, $\omega_i = 0$ and $z_i = 0$, (3.7) and (3.8) model a stationary vehicle.

A state vector x in UAS 2's frame is defined as

$$x = [\widetilde{p}_2^T, \widetilde{\psi}, v_1, \omega_1, \widetilde{z}_2^T]^T \in \mathbb{R}^7, \tag{3.9}$$

where

$$\widetilde{z_2} = R_{\psi_2}^T (z_1 - z_2). \tag{3.10}$$

The state x includes the relative position, heading and wind, and the speeds of UAS 1. Next, the conditions under which x is locally weakly observable are examined when UAS 2 measures the relative position $\widetilde{p_2}$.

Proposition 2: Assume $v_1 \neq 0$ and $\omega_1 \neq 0$. Suppose that Assumption 1 and 2 hold. Then the state x in (3.9) is locally weakly observable given the measurement $\widetilde{p_2}$. ■

Proposition 2 holds independently of the value of v_2, ω_2 or z_2. Thus, UAS 2 can be stationary. Comparing Proposition 2 with Proposition 1 , it is noticed that in the presence of the disturbance, UAS 1 must maintain a non-zero ω_1 to ensure the observability of x. To see why $\omega_1 \neq 0$ is a necessary condition, consider a simplified system where UAS 2 is stationary at $(0, 0)$ and measures the position of UAS 1. Then $\widetilde{p_2} = p_1$. Because p_1 is measured, $\dot{p}_1$ is known and it follows from (3.7) that $v_1[c_{\psi_1} \ s_{\psi_1}]^T + z_1$ is known. Suppose that $\omega_1 = 0$. Then ψ_1 is an unknown constant, which means that $v_1[c_{\psi_1} \ s_{\psi_1}]^T$ is an unknown constant vector. Since z_1 is also unknown and only $z_1 + v_1[c_{\psi_1} \ s_{\psi_1}]^T$ is known, it is impossible to distinguish the two unknown constant vectors z_1 and $v_1[c_{\psi_1} \ s_{\psi_1}]^T$. Thus, $\omega_1 \neq 0$ is a necessary condition for the observability of x.

Proof: Derive the dynamics of x in (3.9). Using (3.5), (3.4) and (3.7), obtain the kinematics of $\widetilde{p_2}$

$$\dot{\widetilde{p_2}} = R_{\psi_2}^T \dot{\widetilde{p}} + \dot{R}_{\psi_2}^T \widetilde{p} = R_{\psi_2}^T (\dot{p_1} - \dot{p_2}) + \dot{R}_{\psi_2}^T R_{\psi_2} \widetilde{p_2}, \tag{3.11}$$

$$= R_{\psi_2}^T \left(v_1 \begin{bmatrix} c_{\psi_1} \\ s_{\psi_1} \end{bmatrix} - v_2 \begin{bmatrix} c_{\psi_2} \\ s_{\psi_2} \end{bmatrix} \right) + R_{\psi_2}^T (z_1 - z_2) + \omega_2 \begin{bmatrix} 0 & 1 \\ -1 & 0 \end{bmatrix} \widetilde{p_2}, \tag{3.12}$$

$$= v_1 \begin{bmatrix} c_{\tilde{\psi}} \\ s_{\tilde{\psi}} \end{bmatrix} - v_2 \begin{bmatrix} 1 \\ 0 \end{bmatrix} + \widetilde{z_2} + \omega_2 \begin{bmatrix} 0 & 1 \\ -1 & 0 \end{bmatrix} \widetilde{p_2}. \tag{3.13}$$

The kinematics of $\widetilde{z}$ is given by

$$\dot{\widetilde{z_2}} = \omega_2 \begin{bmatrix} 0 & 1 \\ -1 & 0 \end{bmatrix} \widetilde{z_2}. \tag{3.14}$$

Thus, obtain the dynamics of x as

$$\dot{x} = f(x) = \begin{bmatrix} \omega_2 x_2 + c_{x_3} x_4 - v_2 + x_6 \\ -\omega_2 x_1 + s_{x_3} x_4 + x_7 \\ x_5 - \omega_2 \\ 0 \\ 0 \\ \omega_2 x_7 \\ -\omega_2 x_6 \end{bmatrix}. \tag{3.15}$$

Since UAS 2 measures $\widetilde{p_2}$, the measurement equation is given by:

$$y = \widetilde{p_2} = \begin{bmatrix} x_1 & x_2 \end{bmatrix}^T = Hx, \tag{3.16}$$

where

$$H = \begin{bmatrix} 1 & 0 & 0 & 0 & 0 & 0 & 0 \\ 0 & 1 & 0 & 0 & 0 & 0 & 0 \end{bmatrix}. \tag{3.17}$$

To analyze the observability of x given y, nonlinear observability rank condition [17] is used to determine if the system is locally weakly observable. Specifically, the matrix ℓ_k is calculated which is given by:

$$\ell_k = \begin{bmatrix} L_f^0 y \\ L_f^1 y \\ \vdots \\ L_f^k y \end{bmatrix}, \tag{3.18}$$

where $L_f^0 y = y$ and $L_f^i y = \frac{\partial}{\partial x}[L_f^{i-1} y] f(x)$, $i = 1, \cdots, k$. Then, iteratively calculate $\dfrac{\partial \ell_k}{\partial x}$ until a full rank matrix is obtained. In that case, x is locally weakly observable.

First, calculate

$$L_f^1 y = \begin{bmatrix} \omega_2 x_2 + c_{x_3} x_4 - v_2 + x_6 \\ -\omega_2 x_1 + s_{x_3} x_4 + x_7 \end{bmatrix}, \tag{3.19}$$

and obtain

$$\frac{\partial \ell_1}{\partial x} = \begin{bmatrix} 1 & 0 & 0 & 0 & 0 & 0 & 0 \\ 0 & 1 & 0 & 0 & 0 & 0 & 0 \\ 0 & \omega_2 & -s_{x_3} x_4 & c_{x_3} & 0 & 1 & 0 \\ -\omega_2 & 0 & c_{x_3} x_4 & s_{x_3} & 0 & 0 & 1 \end{bmatrix}, \tag{3.20}$$

which is rank 4 if x_4 is non-zero. Proceed to calculating $L_f^2 y$

$$\frac{\partial L_f^2 y}{\partial x} = \begin{bmatrix} -\omega_2^2 & 0 & x_4 c_{x_3}[2\omega_2 - x_5] & s_{x_3}[2\omega_2 - x_5] & -x_4 s_{x_3} & 0 & 2\omega_2 \\ 0 & -\omega_2^2 & x_4 s_{x_3}[2\omega_2 - x_5] & -c_{x_3}[2\omega_2 - x_5] & x_4 c_{x_3} & -2\omega_2 & 0 \end{bmatrix}, \tag{3.21}$$

and obtain from (3.20) and (3.21) that

$$\frac{\partial \ell_2}{\partial x} = \begin{bmatrix} 1 & 0 & 0 & 0 & 0 & 0 & 0 \\ 0 & 1 & 0 & 0 & 0 & 0 & 0 \\ 0 & \omega_2 & -s_{x_3} x_4 & c_{x_3} & 0 & 1 & 0 \\ -\omega_2 & 0 & c_{x_3} x_4 & s_{x_3} & 0 & 0 & 1 \\ -\omega_2^2 & 0 & x_4 c_{x_3}[2\omega_2 - x_5] & s_{x_3}[2\omega_2 - x_5] & -x_4 s_{x_3} & 0 & 2\omega_2 \\ 0 & -\omega_2^2 & x_4 s_{x_3}[2\omega_2 - x_5] & -c_{x_3}[2\omega_2 - x_5] & x_4 c_{x_3} & -2\omega_2 & 0 \end{bmatrix}, \tag{3.22}$$

which is rank 6 if x_4 in non-zero. Now, calculate $L_f^3 y$ and obtain

$$\frac{\partial L_f^3 y}{\partial x} = \begin{bmatrix} 0 & -\omega_2^3 & -x_4 s_{x_3} a & -c_{x_3} a & x_4 c_{x_3}[3\omega_2 - 2x_5] & -3\omega_2^2 & 0 \\ \omega_2^3 & 0 & -x_4 c_{x_3} a & -s_{x_3} a & x_4 s_{x_3}[3\omega_2 - 2x_5] & 0 & -3\omega_2^2 \end{bmatrix}, \tag{3.23}$$

where

$$a = 3\omega_2^2 - 3\omega_2 x_5 + x_5^2. \tag{3.24}$$

It is obtained from (3.22) and (3.23)

$$\frac{\partial \ell_3}{\partial x} = \tag{3.25}$$

$$\begin{bmatrix} 1 & 0 & 0 & 0 & 0 & 0 & 0 \\ 0 & 1 & 0 & 0 & 0 & 0 & 0 \\ 0 & \omega_2 & -s_{x_3} x_4 & c_{x_3} & 0 & 1 & 0 \\ -\omega_2 & 0 & c_{x_3} x_4 & s_{x_3} & 0 & 0 & 1 \\ -\omega_2^2 & 0 & x_4 c_{x_3}[2\omega_2 - x_5] & s_{x_3}[2\omega_2 - x_5] & -x_4 s_{x_3} & 0 & 2\omega_2 \\ 0 & -\omega_2^2 & x_4 s_{x_3}[2\omega_2 - x_5] & -c_{x_3}[2\omega_2 - x_5] & x_4 c_{x_3} & -2\omega_2 & 0 \\ 0 & -\omega_2^3 & -x_4 s_{x_3} a & -c_{x_3} a & x_4 c_{x_3}[3\omega_2 - 2x_5] & -3\omega_2^2 & 0 \\ \omega_2^3 & 0 & -x_4 c_{x_3} a & -s_{x_3} a & x_4 s_{x_3}[3\omega_2 - 2x_5] & 0 & -3\omega_2^2 \end{bmatrix}. \tag{3.26}$$

Further calculate

$$\begin{aligned} &\det\left(\frac{\partial \ell_3}{\partial x}^T \frac{\partial \ell_3}{\partial x}\right) \\ &= x_4^4 x_5^6 \left((\omega_2^3 - \omega_2^2 x_5)^2 + (3\omega_2^2 - 2\omega_2 x_5)^2 + (3\omega_2 + x_5)^2 + 1\right), \end{aligned} \tag{3.27}$$

which is non-zero if x_4 (v_1) and x_5 (ω_1) are non-zero. Thus, $\dfrac{\partial \ell_3}{\partial x}$ is rank 7, which proves that x is locally weakly observable given the measurement y. ■

3.1.2 Relative heading estimation with target tracking

In the previous section, observability conditions are developed when UAS 1 has a constant ω_1. However, when UAS 1 tracks a stationary target on the ground, its own control counteracts the disturbance and results in a time-varying ω_1. For example, in [27], the authors develop a feedback method of target tracking using image plane target movement in a side mounted camera. To ensure that the target is in the camera field of view in the presence of a constant wind, the feedback control generates a non-constant heading rate and results in an elliptical tracking path.

In this section, it is assumed that UAS 1 uses the control in [27] to track a target and analyze the observability of relative heading given the relative position measurements in UAS 2's frame. First, briefly review the control in [27]. Let ρ be the range-to-target and η be the bearing-to-target, both from UAS 1. The wind disturbance z_i is parameterized by its magnitude $v_{i\omega} \in \mathbb{R}_{\geq 0}$ and angle $\gamma_i \in \mathbb{S}^1$, i.e.,

$$z_i = v_{iw} \begin{bmatrix} c_{\gamma_i} \\ s_{\gamma_i} \end{bmatrix}. \tag{3.28}$$

The closed-loop tracking dynamics of UAS 1 described in [27] is given by

$$\dot{p_1} = v_1 \begin{bmatrix} c_{\psi_1} \\ s_{\psi_1} \end{bmatrix} + v_{1w} \begin{bmatrix} c_{\chi_1} \\ s_{\chi_1} \end{bmatrix}, \tag{3.29}$$

$$\dot{\rho} = -v_1 s_\eta - v_{1w} s_{\eta+\chi_{1w}-\psi_1}, \tag{3.30}$$

$$\dot{\eta} = \dot{\psi}_1 - \frac{v_1}{\rho} c_\eta - \frac{v_{1w}}{\rho} c_{\eta+\chi_{1w}-\psi_1}, \tag{3.31}$$

$$\dot{\psi}_1 = \frac{v_1}{\rho} c_\eta + \frac{v_{1w}}{\rho} c_{\eta+\chi_{1w}-\psi_1} - k_1 \eta + \nu, \tag{3.32}$$

where $k_1 > 0$ and ν is a signal to minimize the average value of ρ. Set $\nu = 0$.

Substituting the control (3.32) into (3.31), obtain $\dot{\eta} = -k_1 \eta$, which means that the bearing to the target converges to zero. It is further assumed that UAS 1 is tracking the target at the steady state i.e., $\eta = 0$. Equations (3.30)–(3.32) are reduced to

$$\dot{\rho} = -v_{1w} s_{\chi_{1w}-\psi_1}, \tag{3.33}$$

$$\eta = 0, \tag{3.34}$$

$$\dot{\psi}_1 = \frac{v_1}{\rho} + \frac{v_{1w}}{\rho} c_{\chi_{1w}-\psi_1}. \tag{3.35}$$

Given the expression of $\dot{\psi}_1$ in (3.35), let

$$x_7 = v_{1w} c_{\chi_{1w} - \psi_1}, \tag{3.36}$$

and

$$x_8 = v_{1w} s_{\chi_{1w} - \psi_1}. \tag{3.37}$$

Let $x_9 = \rho$. Note that

$$\dot{\psi}_1 = \frac{x_4 + x_7}{x_9} \tag{3.38}$$

and

$$\dot{x}_9 = -x_8. \tag{3.39}$$

The state vector x is defined as

$$x = [\widetilde{p}_2^T, \widetilde{\psi}, v_1, \widetilde{z}^T, x_7, x_8, x_9]^T \in \mathbb{R}^9, \tag{3.40}$$

and derive its dynamics assuming that UAS 1 performs target tracking according to (3.29) and (3.33)–(3.35). Taking the derivative of (3.36) and (3.37) and using (3.38) lead to

$$\dot{x}_7 = v_{1w} s_{\chi_{1w} - \psi_1} \dot{\psi}_1 = x_8 \Big(\frac{x_4 + x_7}{x_9} \Big), \tag{3.41}$$

$$\dot{x}_8 = -v_{1w} c_{\chi_{1w} - \psi_1} \dot{\psi}_1 = -x_7 \Big(\frac{x_4 + x_7}{x_9} \Big). \tag{3.42}$$

Then the dynamics of x is given by

$$\dot{x} = f(x) = \begin{bmatrix} \omega_2 x_2 + c_{x_3} x_4 - v_2 + x_5 \\ -\omega_2 x_1 + s_{x_3} x_4 + x_6 \\ \frac{x_4 + x_7}{x_9} - \omega_2 \\ 0 \\ \omega_2 x_6 \\ -\omega_2 x_5 \\ x_8 (\frac{x_4 + x_7}{x_9}) \\ -x_7 (\frac{x_4 + x_7}{x_9}) \\ -x_8 \end{bmatrix}. \tag{3.43}$$

Proposition 3: Suppose that Assumption 2 holds. Assume that v_1 is a positive constant. The state x in (3.43) is locally weakly observable given the measurement $\widetilde{p_2}$. ■

Proposition 2 is significant because *i)* no motion constraint on UAS 2 is required, i.e., v_2 and ω_2 can be zero; *ii)* not only $\widetilde{\psi}$ and v_1 are observable, ρ is also observable, which means that UAS 2 can estimate the position of the ground target without observing the target.

Proof: The relative kinematics is given by (3.43) and the measurement equation is given by

$$y = \widetilde{p_2} = Hx, \tag{3.44}$$

where

$$H = \begin{bmatrix} 1 & 0 & 0 & 0 & 0 & 0 & 0 & 0 & 0 \\ 0 & 1 & 0 & 0 & 0 & 0 & 0 & 0 & 0 \end{bmatrix}. \tag{3.45}$$

Calculate the Lie derivatives according to (3.18). Since the dimension of x and y is 9 and 2, respectively, calculate the Lie derivatives up to $k = 4$ and obtain $\frac{\partial \ell_4}{\partial x}$.Using Matlab symbolic toolbox, it is verified that $\frac{\partial \ell_4}{\partial x}$ is rank 9, which proves the state observability given the $\widetilde{p_2}$ measurement. In particular, the rank of $\frac{\partial \ell_4}{\partial x}$ evaluated at $v_2 = 0$ and $\omega_2 = 0$ is also 9. Thus, the state x is observable even if either v_2 or ω_2 is zero. ■

A simpler scenario is when UAS 2 is stationary, i.e., $v_2 = 0$, $\omega_2 = 0$, and $z_2 = 0$. In this case, the state vector x in (3.40) is reduced to

$$x = [\widetilde{p_2}^T, \widetilde{\psi}, v_1, z_1^T, \rho]^T \in \mathbb{R}^7. \tag{3.46}$$

Proposition 4: Suppose that Assumption 2 holds. Assume that v_1 is a positive constant. The state x in (3.46) is locally weakly observable given the measurement $\widetilde{p_2}$. ■

Proof: Obtain the dynamics of x by simplifying (3.43) with $v_2 = 0$, $\omega_2 = 0$, and $z_2 = 0$

$$\dot{x} = \begin{bmatrix} c_{x_3} x_4 + x_5 \\ s_{x_3} x_4 + x_6 \\ \frac{(x_4 + x_5 c_{x_3} + x_6 s_{x_3})}{x_7} \\ 0 \\ 0 \\ 0 \\ x_6 c_{x_3} - x_5 s_{x_3} \end{bmatrix}. \tag{3.47}$$

The measurement equation is given by (3.44).

Using (3.18), calculate the Lie derivatives up to $k = 3$ and obtain $\text{rank}\left(\frac{\partial \ell_3}{\partial x}\right) = 7$ using Matlab symbolic toolbox. Thus, x is locally weakly observable. In particular, when $z_1 = 0$,

$$\det\left(\frac{\partial \ell_3}{\partial x}^T \frac{\partial \ell_3}{\partial x}\right) = (x_4^{14} + x_4^{12} x_7^2)/x_7^{12}, \tag{3.48}$$

which is positive if $x_4 \neq 0$. ■

3.1.3 Simulation results

In this section, a simulation example of Proposition 4 is presented to illustrate that the state can be estimated based on the observability result. Consider a ground station located at $(0,0)$ meters in the $x-y$ plane. UAS 1 starts at $(200,200)$ meters with the heading along the positive x axis and tracks a ground target located at $(200,300)$ meters. Thus, the initial range to the target is 100 meters. The wind velocity is $(0,5)$ m/s. The scenario is shown in Fig. 3.1. The ground station measures the position of UAS 1 by fusing range and

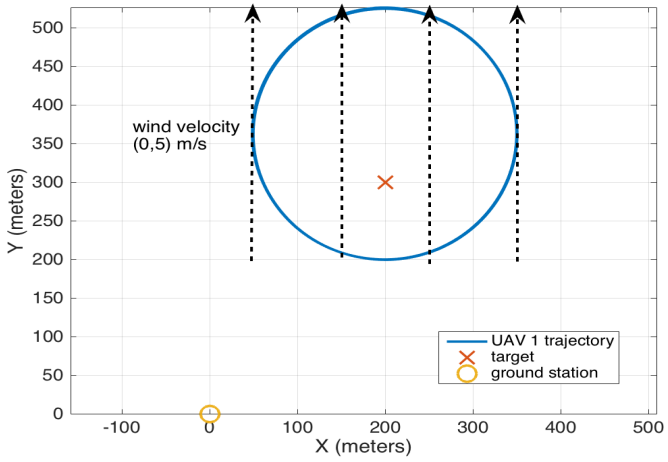

Figure 3.1: UAS 1 is tracking a ground target in the presence of wind (2D view). The wind direction is marked with the dashed arrows. The wind velocity is $(0,5)$ m/s. The ground station measures the position of UAS 1.

azimuth angle measurements of the UAS. The noise associated with the range and azimuth measurements is modeled as zero mean Gaussian noise with a standard deviation of σ_r meters and σ_a degrees, respectively. At time kT, let the azimuth and range measurements be $a(k)$ and $r(k)$, respectively. Then the relative position measurement is given by

$$\hat{y}(k) = r(k)[c_{a(k)} \; s_{a(k)}]^T, \tag{3.49}$$

whose uncertainty is approximated by

$$\Sigma_p(k) = \begin{pmatrix} c_{a(k)} & -s_{a(k)} \\ s_{a(k)} & c_{a(k)} \end{pmatrix} \begin{pmatrix} \sigma_r^2 & 0 \\ 0 & r(k)^2\sigma_a^2 \end{pmatrix} \begin{pmatrix} c_{a(k)} & s_{a(k)} \\ -s_{a(k)} & c_{a(k)} \end{pmatrix}. \tag{3.50}$$

Note that $\Sigma_p(k)$ varies with $r(k)$ and $a(k)$. In the simulation, choose $\sigma_a = 0.2\pi/180$ rad and $\sigma_r = 5$ meters. The sampling time is 0.05 seconds.

An extended Kalman filter (EKF) [29] is designed to estimate x in (3.46) using the position measurements of UAS 1. The initial estimate of UAS 1's position is given by the first measurement of the UAS and its

covariance is given in (3.50). The initial heading estimate is generated randomly between 0 rad and 2π rad with its variance equal to $\frac{(2\pi)^2}{12}$. The initial speed estimate is set to 8 m/s with a variance 5. The initial wind estimate is $(0,0)$ m/s with a covariance matrix $5I_2$. The initial estimate of the range between the target and the UAS is 50 m with a variance of 30.

Fig. 3.2–3.4 show that the estimates of UAS 1's speed, the wind, UAS 1's heading, and the range between UAS 1 and the target converge to the truth, respectively. Since UAS 1's position is measured and the range between UAS 1 and the target can be estimated, the ground station can estimate the position of the target without actually observing the target.

Figure 3.2: The speed of the UAS estimated at the ground station converges to the true speed of the UAS.

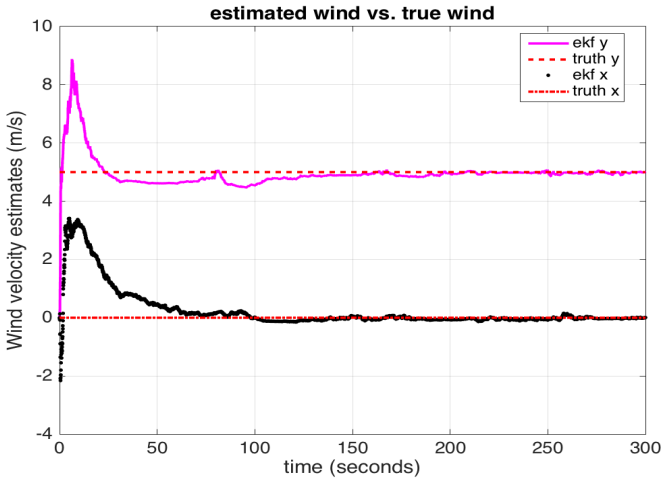

Figure 3.3: The estimated wind velocity in the x and y directions converges to the true velocity.

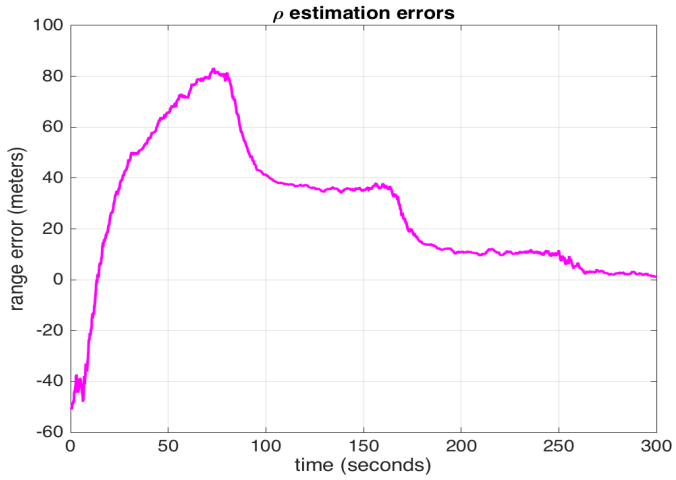

Figure 3.4: The estimation error between ρ and the estimated ρ converges to zero..

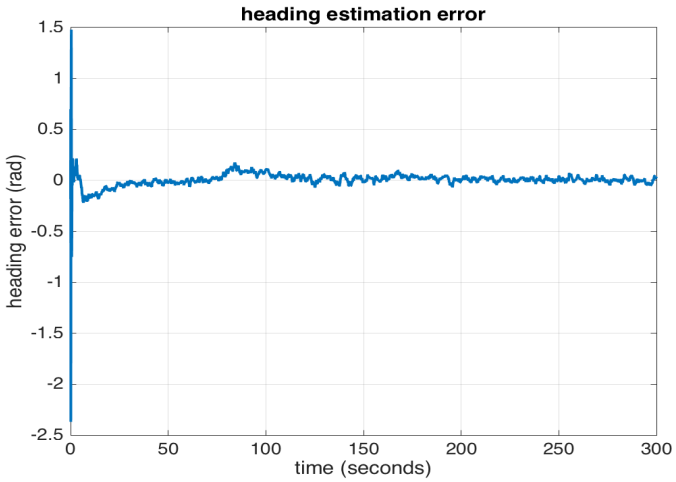

Figure 3.5: The estimation error between the true heading ψ_1 and the estimated heading converges to zero.

3.2 Observability Properties of Relative State Estimation with Bearing-Only Measurements

In denied environments, it is possible to use relative measurements between vehicles to perform relative state estimation and localization [19, 30]. For two-vehicle relative localization, [22] analyzes the observability of the relative states given four types of relative measurements: relative orientation, relative range, and two kinds of relative bearing. In [28], the authors extend the observability analysis in [22] from two-vehicle scenarios to multi-vehicle scenarios with bearing-only measurements. In [10], observability of the relative state in 3D is analyzed.

For the observability results in [10, 22, 28] to hold, the linear and angular velocities of the vehicles must be time-varying and constantly exchanged between vehicles. Such an assumption does not hold for non-cooperative vehicles or in denied environments, where communication bandwidth is limited. Therefore, it is important to understand observability properties of the relative state between the vehicles in the absence of communication. In [3], the observability rank condition [17] is employed and it is shown that if vehicle 2 measures the relative position to vehicle 1, the linear speed and angular velocity of vehicle 1 and the relative heading between the two vehicles are locally weakly observable without communication. In [2], the analysis in [3] is extended to scenarios with disturbances.

Observability properties of relative state estimation between two vehicles are investigated in bearing-only scenarios. It is assumed that one vehicle, say vehicle 2, is equipped with a monocular camera sensor and measures the bearing (azimuth) angles of vehicle 1. This is more challenging than the scenarios considered in [2,3], where relative position measurements are available. Because of the nonlinear bearing measurements, applying the observability rank condition results in a complicated observability matrix. It is possible to obtain the generic rank of the observability matrix from Matlab. However, it remains difficult to understand scenarios in which the observability matrix loses rank.

Instead, *global* observability [7, 17] of the relative state estimation problem is investigated. Given measurements $y(t)$, conditions under which a *unique* initial condition of the relative state exists is examined. Global observability is weaker than local observability since the states do not need to be distinguished locally or in a small time interval [17]. Thus, global observability is easier to achieve. In addition, analyzing global observability allows us to obtain unobservable conditions. These conditions should be avoided in practice to ensure consistent and stable estimates of the relative state.

It is assumed that the angular velocities and linear speeds of the two vehicles are constant and consider four scenarios where each of the vehicles can be orbiting or cruising. In Section 3.2.1, vehicle 1 to communicate its linear speed and angular velocity to vehicle 2 is allowed. Even with communication, it is proved that there are unobservable scenarios, particularly when both vehicles are cruising or orbiting with the same angular

velocity. An interesting finding is that in these unobservable scenarios, vehicle 2 moves with a greater linear speed than vehicle 1.

In Section 3.2.2, observability properties without communication between the vehicles are analyzed. When both vehicles move with constant velocities, it is well known that the range between the vehicles is not observable [25]. When vehicle 2 moves with a constant velocity and vehicle 1 is orbiting, it is proved that the relative state is observable. It is also prove that when both vehicles are orbiting, the relative state is generally observable. However, when the angular velocities of both vehicles are the same, the relative state is not weakly observable, implying that no estimator can provide stable and consistent estimates of the relative state. The proofs for the observability results are presented in Appendix A

3.2.1 Cooperative bearing-only scenarios

A. Relative kinematics

Consider the model of two vehicles as defined in Section **??**. It is assumed that vehicle 1 is cooperative and sends its ω_1 and v_1 information to vehicle 2 with negligible delays. Define the relative state vector $x \in \mathbb{R}^3$ as

$$x = [\tilde{p}_2^T, \tilde{\theta}]^T, \tag{3.51}$$

and obtain its kinematics from (3.1)- (3.2) as

$$\dot{x} = \begin{pmatrix} \omega_2 x_2 + c_{x_3} v_1 - v_2 \\ -\omega_2 x_1 + s_{x_3} v_1 \\ \omega_1 - \omega_2 \end{pmatrix}, \tag{3.52}$$

where x_i is the ith element of x.

Observability properties of x when vehicle 2 measures the relative bearing between the two vehicles are analyzed, e.g., when vehicle 2 has a monocular camera sensor. The measurement model takes the following form

$$y(t) = atan2(\tilde{p}_2^y(t), \tilde{p}_2^x(t)) = atan2(x_2(t), x_1(t)), \tag{3.53}$$

where $\tilde{p}_2^x(t)$ and $\tilde{p}_2^y(t)$ are the x and y component of $\tilde{p}_2$ at time t, respectively, and $atan2(\cdot,\cdot) \in (-\pi, \pi]$ is the arctan function with two arguments that takes into account the sign information of the arguments to return the appropriate quadrant information.

In Section 3.2.1.B, an example where the relative state may not be observable even when v_1 and ω_1 are available to vehicle 2 is provided. In Section 3.2.1.C, observability properties of (3.52) and (3.53) for four common scenarios are analyzed. To develop observability conditions for each scenario, it is assumed that there exist two initial conditions that generate the same set of measurements. Based on the trajectories of the

relative state, conditions under which the two initial conditions are the same are obtained, thereby establishing observability. The observability properties are summarized in Theorem 1 and Table 3.1.

B. A Motivating example

It has been shown in the passive ranging literature (see e.g., [25]) that if vehicle 1 and 2 move with constant velocities and v_1 is unknown to vehicle 2, their range is not observable with only bearing measurements. In this section, scenarios where the range remains unobservable even if vehicle 1 transmits its speed v_1 to vehicle 2 are illustrated. Following assumption is made:

Assumption 1: The bearing measurements $y(t)$ are time-varying. ■

Assumption 1 is reasonable because constant bearing measurements provide no motion information of vehicle 1 and therefore result in an unobservable system.

Consider an example, where vehicle 2 moves with a constant speed of $v_2 > 0$ along the x axis. Without loss of generality, it is assumed that vehicle 2 starts at $(0,0)$. Consider one trajectory of vehicle 1 starting at (a_1, b_1) and moving with a constant speed of $v_1 > 0$ and a constant relative heading $\tilde{\theta}_1 \in [0, 2\pi)$ with respect to vehicle 2. Consider another trajectory of vehicle 1 starting at (a_3, b_3) and moving with the same constant speed v_1 and a constant relative heading $\tilde{\theta}_3 \in [0, 2\pi)$ with respect to vehicle 2. The bearing angles of the two trajectories of vehicle 1 relative to vehicle 2 are given by

$$y_j(t) = atan2(b_j + v_1 s_{\tilde{\theta}_j} t, a_j + v_1 c_{\tilde{\theta}_j} t - v_2 t), \quad j = 1, 3. \tag{3.54}$$

Proposition 1: Suppose that a_1, b_1, a_3, b_3 satisfy

$$\frac{a_1}{a_3} = \frac{b_1}{b_3} = \frac{s_{\tilde{\theta}_1}}{s_{\tilde{\theta}_3}} > 0 \tag{3.55}$$

and v_1, v_2 satisfy

$$v_1 = \frac{s_{\tilde{\theta}_3} - s_{\tilde{\theta}_1}}{s_{\tilde{\theta}_3 - \tilde{\theta}_1}} v_2. \tag{3.56}$$

Then the two trajectories of vehicle 1 yield the same bearing angles relative to vehicle 2, i.e., $y_1(t) = y_3(t)$, where $y_j(t)$, $j = 1, 3$ are defined in (3.54). ■

Proof. Using (3.56),

$$\begin{aligned} \frac{v_1 c_{\tilde{\theta}_1} t - v_2 t}{v_1 c_{\tilde{\theta}_3} t - v_2 t} &= \frac{s_{\tilde{\theta}_3} c_{\tilde{\theta}_1} - s_{\tilde{\theta}_1} c_{\tilde{\theta}_1} - s_{\tilde{\theta}_3 - \tilde{\theta}_1}}{s_{\tilde{\theta}_3} c_{\tilde{\theta}_3} - s_{\tilde{\theta}_1} c_{\tilde{\theta}_3} - s_{\tilde{\theta}_3 - \tilde{\theta}_1}} \\ &= \frac{s_{\tilde{\theta}_1}(c_{\tilde{\theta}_3} - c_{\tilde{\theta}_1})}{s_{\tilde{\theta}_3}(c_{\tilde{\theta}_3} - c_{\tilde{\theta}_1})} = \frac{s_{\tilde{\theta}_1}}{s_{\tilde{\theta}_3}}. \end{aligned} \tag{3.57}$$

Letting $k = \frac{s_{\tilde{\theta}_1}}{s_{\tilde{\theta}_3}}$ and using (3.55) and (3.57),

$$b_1 + v_1 s_{\tilde{\theta}_1} t = k(b_3 + v_1 s_{\tilde{\theta}_3} t) \tag{3.58}$$

$$a_1 + v_1 c_{\tilde{\theta}_1} t - v_2 t = k(a_3 + v_1 c_{\tilde{\theta}_3} t - v_2 t). \tag{3.59}$$

Since $k > 0$, it follows from (3.54), (3.58) and (3.59) that $y_1(t) = y_3(t)$. Therefore, both trajectories yield the same bearing measurements (3.54) for vehicle 2. ■

In the traditional passive ranging literature, the speed v_1 is unknown and there exist an infinite number of trajectories that have the same bearing angles relative to vehicle 2 as vehicle 1's. With the knowledge of v_1, it is shown that the infinite number of trajectories are reduced to those determined by (3.55) and (3.56). Given v_1, v_2 and $\tilde{\theta}_1$, if there exists a solution of $\tilde{\theta}_3$ to (3.55) and (3.56), the two trajectories will have different relative heading and range to vehicle 2 but yield the same bearing measurements. Thus, the relative position and heading between vehicle 1 and 2 are unobservable.

Proposition 2: A solution of $\tilde{\theta}_3$ to (3.55) and (3.56) exists only if $v_1 < v_2$. ■

Proposition 2 is illustrated using a numerical example. The proof is presented in Section A.1. Assume that $\tilde{\theta}_1 = \pi/6$ and $v_1 = v_2$. Then there is no solution of $\tilde{\theta}_3$ that satisfies (3.55) and (3.56). However, when $v_1 < v_2$, say $v_1 = 0.9342 v_2$, a solution of $\tilde{\theta}_3 \approx 0.2527 \neq \tilde{\theta}_1$ exists. Thus, the relative state between the two vehicles is not observable. Fig. 3.6 shows this unobservable scenario.

The existence of a solution to (3.55) and (3.56) depends on $\tilde{\theta}_1$, which is unknown *a priori*. Although the two trajectories of vehicle 1 are isolated in space, an estimator of vehicle 1's trajectory may converge to either of the two trajectories, depending on the initialization of the estimator. In the next section, sufficient conditions for the relative state to be observable are derived. These conditions ensure that no other trajectory can generate the same bearing measurements as vehicle 1. In particular, four scenarios are considered:

i) vehicle 1 and 2 both cruising;

ii) vehicle 1 and 2 both orbiting;

iii) vehicle 2 orbiting and vehicle 1 cruising;

iv) vehicle 1 orbiting and vehicle 2 cruising.

C. Observability results

Theorem 1: Consider the kinematics (3.52) with the measurements in (3.53). Suppose that v_1 and ω_1 are constant and available for vehicle 2 and $v_1 > 0$. Suppose that Assumption 1 holds. The relative state $(\tilde{p}_2, \tilde{\theta})$, $\tilde{\theta} \in [0, 2\pi)$ is observable if

i) $\omega_1 = 0$, $\omega_2 = 0$, and $v_1 \geq v_2$, or

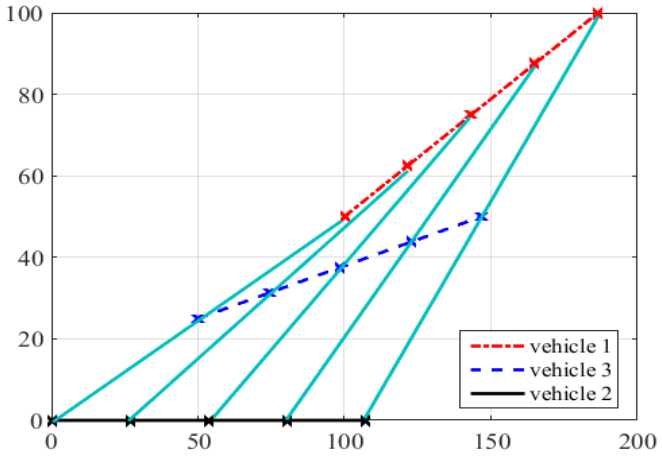

Figure 3.6: An unobservable example where two trajectories of vehicle 1 generate the same set of bearing measurements with respect to vehicle 2. The bearing angles at five sample points are indicated by cyan lines. Vehicle 1 and 2 move with a linear speed of 5 m/s and 5.3523 m/s, respectively. The relative headings of the two trajectories with respect to vehicle 2 are 30 degrees and 14.4775 degrees, respectively.

ii) $\omega_1 \neq 0$, $\omega_2 \neq 0$, $\omega_1 \neq \omega_2$ if $v_1 < v_2$, $\omega_1 \neq 2\omega_2$, $\omega_2 \neq 2\omega_1$, and $v_2 > 0$, or

iii) $\omega_1 = 0$, $\omega_2 \neq 0$, and $v_2 > 0$, or

iv) $\omega_2 = 0$ and $\omega_1 \neq 0$ and $v_2 > 0$. ■

The observability results in Theorem 1 are summarized in Table 3.1 below. It is concluded the observability condition $v_1 \geq v_2$ for case *i)* based on Proposition 2 . For case *iii)*, it has been shown in the traditional passive ranging literature that if vehicle 2 maneuvers and vehicle 1 moves with a constant velocity, the range between them is observable even without the v_1 information. The orbiting motion as the maneuver in case *iii*) is considered. Thus, the relative state is observable. The proofs for case *ii)* and *iv)* are presented in Section A.2.

Table 3.1: Observability results for bearing-only scenarios when $v_1 > 0$, vehicle 1 transmits v_1 and ω_1 to vehicle 2 and Assumption 1 holds.

Observability	$\omega_1 = 0$	$\omega_1 \neq 0$
$\omega_2 = 0$	i) $v_1 \geq v_2$, or $v_2 = 0$	iv) $v_2 > 0$
$\omega_2 \neq 0$	iii) $v_2 > 0$	ii) $\omega_1 \neq \omega_2$ if $v_1 < v_2$, $\omega_1 \neq 2\omega_2$, $\omega_2 \neq 2\omega_1$, $v_2 > 0$

As discussed later in Remark 1 in Section A.2, when $\omega_1 = \omega_2 \neq 0$ and $v_1 < v_2$, an unobservable scenario exists for every initial condition. Fig. 3.7 below shows such an unobservable scenario. For $\omega_1 = 2\omega_2$ or $\omega_2 =$

$2\omega_1$, unobservable scenarios exist only for some specific initial conditions. These conditions for $\omega_1 = 2\omega_2$ in Remark 1 are characterized.

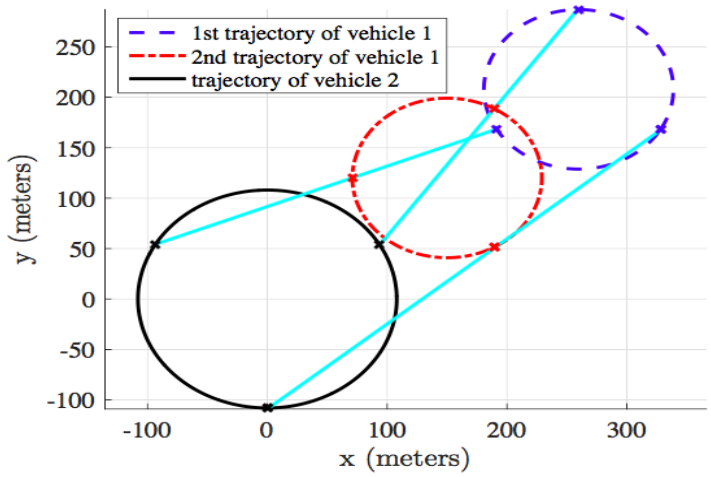

Figure 3.7: An unobservable example where two trajectories of vehicle 1 generate the same set of bearing measurements with respect to vehicle 2. Vehicle 1 and 2 both orbit at 0.215 rad/s. The bearing angles at three sample points are indicated by cyan lines. The two trajectories move with a linear speed of 17 m/s while vehicle 2 moves with a linear speed of 22.2224 m/s. The initial relative headings of the two trajectories with respect to vehicle 2 are 60 degrees and 30 degrees, respectively.

3.2.2 Non-cooperative bearing-only scenarios

Theorem 1 assumes that v_1 and ω_1 are available to vehicle 2. In denied environments or for non-cooperative vehicles, v_1 and ω_1 can be unknown and thus need estimation. It is assumed that v_1 and ω_1 are unknown constants and augment the state x in (3.51) with v_1 and ω_1. Let $x_4 = \omega_1$ and $x_5 = v_1$. The dynamics of the augmented x is given by

$$\dot{x} = \begin{pmatrix} \dot{\tilde{p}}_2 \\ \dot{\tilde{\theta}} \\ \dot{\omega}_1 \\ \dot{v}_1 \end{pmatrix} = \begin{pmatrix} \omega_2 x_2 + c_{x_3} x_5 - v_2 \\ -\omega_2 x_1 + s_{x_3} x_5 \\ x_4 - \omega_2 \\ 0 \\ 0 \end{pmatrix}. \tag{3.60}$$

Next, observability properties of (3.60) and (3.53) are studied for case *i)–iv)*. It is well known from the passive ranging literature that without the knowledge of v_1, case *i)* and *iii)* are unobservable and observable, respectively. Therefore, case *ii)* and *iv)* are focussed.

The scenario in case *iv)* is of particular interest to the target handoff problem [**?**] because vehicle 1 may be orbiting to track a stationary or slowly moving target while vehicle 2 moves towards vehicle 1 and estimates the relative state between the two vehicles. The following observability result establishes that even if ω_1 and v_1 are not transmitted, all the state $(\tilde{p}_2, \tilde{\theta}, \omega_1, v_1)$ is observable:

Proposition 3: Consider the kinematics (3.60) with the measurement in (3.53). Suppose that $\omega_1 \neq 0$, $\omega_2 = 0$, $v_1 > 0$ and $v_2 > 0$. Then the state $(\tilde{p}_2, \tilde{\theta}, \omega_1, v_1)$ in (3.60) is observable. ■

For case *ii)*, the result are as follows:

Proposition 4: Consider the kinematics (3.60) with the measurement in (3.53). Suppose that $\omega_1 \neq 0$, $\omega_2 \neq 0$, $v_1 > 0$ and $v_2 > 0$. Then the relative state $(\tilde{p}_2, \tilde{\theta}, \omega_1, v_1)$ in (3.60) is observable except that

a) if $\omega_1 = \omega_2$, the relative state is not weakly observable for any initial conditions;

b) if $\omega_1 = \omega_2/3$ or $\omega_1 = \omega_2/2$ or $\omega_1 = 2\omega_2/3$ or $\omega_1 = 3\omega_2/2$ or $\omega_1 = 2\omega_2$ or $\omega_1 = 3\omega_2$, the relative state is not observable for some specific initial conditions.

c) if $\omega_1 = -\omega_2$ and $v_1 = v_2$, the relative state is not observable for some specific initial conditions. ■

Proposition 4 shows that the relative state is generally observable in case *ii)* except under specific conditions related to ω_1 and ω_2. The scenario in *a)* should be avoided in practice since no estimator can provide stable and consistent estimates of the relative state. *a*) using the observability rank condition are also verified. The conditions in *b)–c)* present less of an issue than *a*) since unobservable scenarios occur only for specific initial conditions. Compared with the conditions of case *ii)* in Table 3.1, additional unobservable conditions appear in *b)–c)* due to the unknown ω_1 and v_1.

The proofs for Proposition 3 and 4 are presented in Appendix A.

Chapter 4

EXPERIMENTAL SETUP

4.1 Hardware

4.1.1 Optitrack Motion Capture System

Multiple cameras, calibration tools and other components make up a motion capture system setup. The correctly mounted cameras and other devices ensure that the cameras are able to capture all the necessary movements of the object which improves the tracking capabilities of the motion tracking system. An optimized capture volume provides good system performance and accuracy and overcomes the marker occlusions and mislabeling issues. Thus, a well-configured setup can save a significant amount of time and effort in data post-processing. The detail of some important components of Optitrack motion capture system is provided below [9]

Prime 17W Cameras

The prime 17W cameras as shown in Fig. 4.1 are wide angle cameras that provides edge-to-edge coverage across the camera's image sensor. It has an amazing 70 degree horizontal field of view and 40 degrees vertical field of view with upto 360 frames per second capture rate and a resolution of 1.7 megapixels.
The set up of Prime 17W cameras is easy as they are connected through the ethernet. It provides an extensive cabling range of up to 300 feet and a good bandwidth capabilities. The are low powered cameras which uses almost 25W of power. It has been observed that some wide angle cameras which are used to capture motion are vulnerable to vignetting on their eges that adversely affect the camera's coverage capabilities. State-of-the-art prime 17W cameras do not face such problems. These cameras also have different camera control features which enhance the overall performance of the motion capture system. Some are listed below

- Image processing type
- Frame rate
- Exposure
- Threshold

Figure 4.1: Optitrack Prime 17W Camera [9]

- Illumination
- Status LED control

Netgear Prosafe 24-port ethernet switch are used. The 8 cameras used in the lab are connected through this switch. Overall, this switch has the capability to support up to 12 Prime 17W ethernet cameras.

Calibration Tools

Calibration tools required to properly initialize the Motive capture software are calibration wand and calibration square. Their use and description has been defined below

Calibration Wand CWM 250

The Calibration Wand CWM 250 as shown in Fig. 4.2 is a Micron Series wand is an aluminum wand which is designed for precise calibration of medium to large capture volumes. The wand remained calibrated through a wide range of temperature as they are usually made up of a material with a low coefficient of thermal expansion. It has a calibration accuracy of around 2 microns.

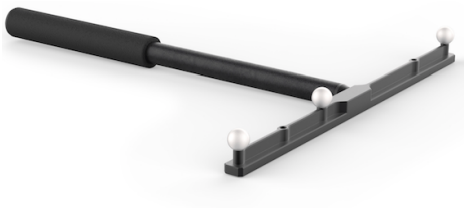

Figure 4.2: Optitrack Calibration Wand CWM 250 [9]

The CW-250 Calibration Wand Kit includes the following items

- Markers - 3x12.7 mm (1/2”)
- Spacing - 250 mm
- Wand Handle: ¼-20 mount
- Handle extension thread
- Adjustable wand position

Calibration Square CS 100

Calibration square as shown in Fig. 4.3 is used to set the ground plane. It has been standardized on a Right-Handed Coordinate System.

Figure 4.3: Optitrack Calibration Square CS 100 [9]

Motion Capture Markers

Motion capture markers as shown in Fig. 4.4 are highly reflective spherical markers which are used for better visualization of a body whose movement is supposed to be captured by the motion capture cameras. In motive software, a group of markers on a body is grouped together to make it a rigid bosy. Then, all the camera detect the movement of a group of markers as movement of one body.

The marker size affects the visibility of the object being tacked. Larger markers are able to stand out in the camera view and can be tracked from a longer distance. These big markers are not good for capturing fine movements. On the other hand, small markers are used for precise facial tracking and small objects but not good for tracking from long distances.

Figure 4.4: Motion Capture Markers with adhesive [9]

License Key USB

To run the Motive software, an activated license information is required. Along with the activated license, a license file is also required to be installed inside the PC for the Motive software to work. For this purpose, a Hardware key or a dongle as shown in Fig. 4.5 is used which has the necessary software file to run the Motive software, allowing one license to be used on multiple computers. Motive software can not run with out a hardware key.

Figure 4.5: Motion Capture Software Hardware Key [9]

4.1.2 Optitrack Hardware Setup

To set up the Optitrack motion track hardware, the minimum requirement is to have the hardware as described in section 4.1.1. Other than that, ethernet cables are also needed for connecting cameras, a frame to mount cameras at different position which would enable us to capture the maximum details of the whole capture volume.

Camera placement

For 3D tracking of orientation and position of a body, the camera should be placed at the boundaries of the capture volume. This ensures that the cameras are able to properly overlapping with one another to cover all the area and minimizes the wastage of camera coverage. A few important points to consider before mounting the camera are listed below:

1. The cameras should be mounted at one of the highest points in the desired capture area. The cameras should be distributed equidistantly around the area.

2. The motion capture markers enable the cameras to see the object in 2D. These marker positions are triangulated to compute the 3D position of each marker. Thus, it is advised to place proper number of markers at specific places on the object which covers almost the whole body of the object. It allows the triangulation algorithm to properly calculate the 3D image of the object which helps the accuracy of the object tracking.

3. Camera-to-camera distance should also be consistence to prevent occlusion and errors in reconstruction calculations.

4. Camera-to-object distance may vary for different types of capture applications. The long distances provides enough coverage to capture large capture areas whereas short distances will give less camera coverage but a more accurate tracking measurement.

5. Placing cameras at high elevation is suggested so that it can cover all the capture area. It is also seen that cameras with varying altitudes are mounted. It provides different viewing angles from different heights.

Wiring and Connections

The motion track camera Prime 17W is an ethernet camera and the network of multiple cameras is created through ethernet cables which are also used to interface with the host PC. All the cameras are connected together a Netgear Prosafe 24-port ethernet switch as shown in Fig. 4.6. The ouput of this switch is connected to the host PC which communicates all the information of cameras to the motion capture software Motive. Different ethernet cables are commercially available which has different specifications. for data transfer rate . Cat6e, Cat6 and Cat7 are recommended for 10 gigabit uplink switch. The ethernet cables offer faster data transfer rates as well as longer distance capabilities i.e., upto 100m.

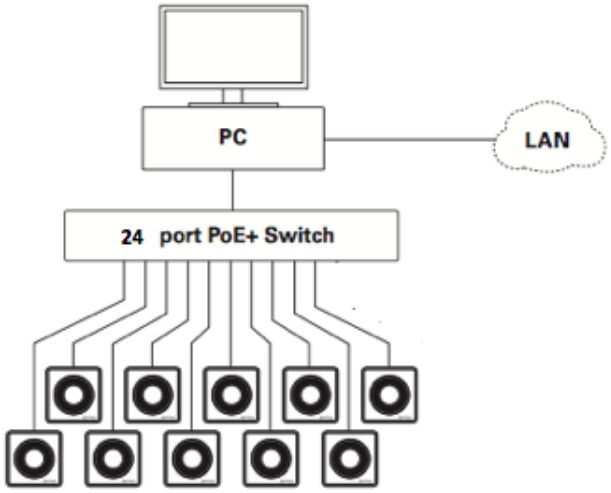

Figure 4.6: Camera Ethernet Network [9]

4.1.3 Parrot AR 2.0 Drone

The Parrot AR.Drone 2.0 as shown in Fig. 4.7 is an automatic piloting drone which makes the take-off and landing very easy. It allows drone flips with a single button. The actuators of the Parrot AR drone has 4 brushless motors, each with a power of 14.5 watts and a revolution capacity of 28,500 revolutions per minute. They are equipped with a lithium polymer (LiPo) battery of 1000mAh capacity. The embedded linux system in this drone has the ARM Cortex A8, 32-bit processor with high-speed USB 2.0 for extensions. They are connected with mobile applications and other workstation though wifi network. They are different internal and external sensors for measuring the physical quantities around it during the flight. They are equipped with gyroscope which has an accuracy of 2,000' per second, an accelerometer with an accuracy of close to 50 mg, a magnetometer which has an accuracy of 6°, and a pressure sensor whose accuracy of around 10 Pa They have the HD recording capabilities and has a front camera of 720p, 30FPS. They have a vertical VGA camera with 60 FPS to measure the ground speed.

4.2 Software

4.2.1 Motive Software

Motive software is designed to track object for the motive motion capture systems. It allows calibration of the system and provides user with the option to calibrate the hardware according to their needs so that the overall system can be used to capture and process 3D data. With the help of the motion capture markers, it

Figure 4.7: Parrot AR 2.0 Drone [9]

combines all the markers to form a rigid body or a skeleton and provides the user with 6 DOF (3D position and orientation).

Camera Calibration

Once the software is installed and all the licenses are activated, calibration and integration of hardware with the motive software is done. Camera calibration of motive motion capture system is one of the most essential parts to get the best tracking results from this system. During calibration, the cameras assess the position and orientation of the object with respect to all the cameras. They calculate the distortion in the captured frames and construct a 3D capture area through triangulation.
The different steps involved in camera calibration are as follows:

Masking

The unnecessary reflections and markers should be removed to the maximum extent before the calibration of the motion capture system is done. In the worst case, the software would deny to calibrate the motion capture cameras if the camera is having too many reflections or errors because it would degrade the results of the object tracking. In some cases, these reflections and errors could not be adjusted through simple calibration changes. Then, these are ignored using a masking tool. This tool masks the certain pixels of the camera where errors are present. It should be noted that masking exceeding a certain number of pixels would result in inaccurate tracking results. It must be noted that the camera is not taking in the values where the camera masking is applied. It may result on occlusion of data if more than necessary pixels are masked and our object is continuously lying in the masked area.

Wanding

The process of wanding involves waving of wand infront of the camera for a certain period of time till the camera capture system captures sufficient values.These values are use to compute the respective position and

orientation of the in the 3D space. It is recommended to cover the camera area where the object is supposed to move otherwise, the cameras wont be able to capture the object motion.

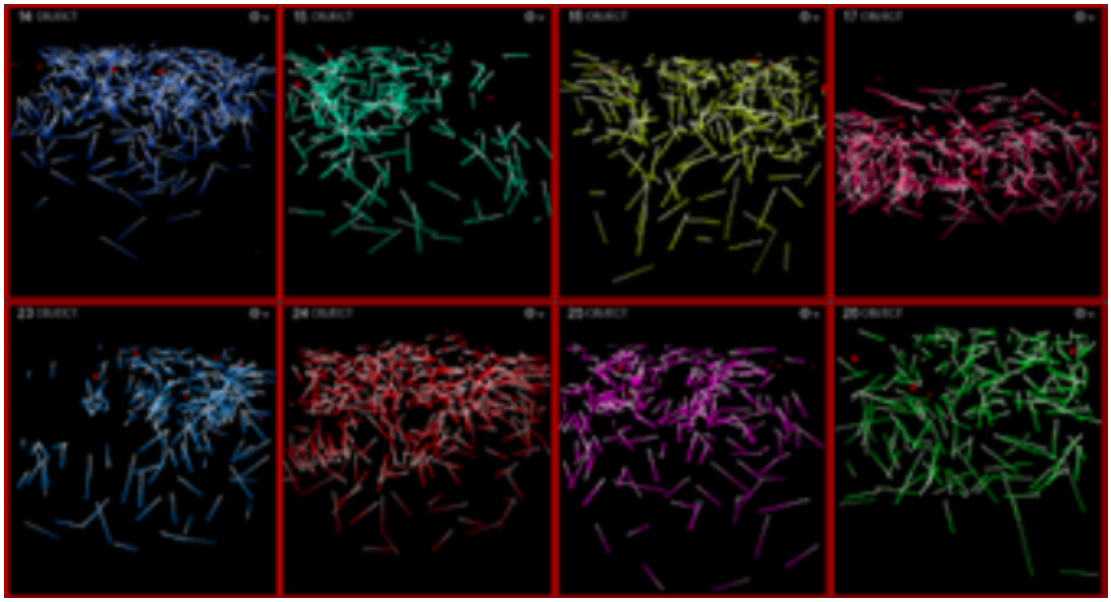

Figure 4.8: Wanding Results [9]

Once wanding is done and it has been established that enough readings have been obtained as shown in Fig. 4.8, calibration calculation is done where the software assesses the quality of the calibration. If too much of masking is done and insufficient wanding data is obtained, the software may not allow to finish the system calibration. It may ask for some other steps to improve the calibration quality before motion capturing is started.

Ground Plane and Origin

The last calibration step is to adjust the ground plane and the origin. It is achieved by using the calibration square. It is placed in the capture area of interest where lately wanding has been done. The exact place of the calibration square will be defined as the origin. The longer length of the calibration square will be referenced as z-axis and smaller length as x-axis. As per right hand coordinate system, the vertical length will automatically be defined as the y-axis.

Rigid Body Tracking

After camera calibration and origin adjustment, a rigid body is created with the help of retroreflective markers to combine all the markers as one object. In this way, these individual markers are treated as a single body and can easily be tracked. The position and orientation of object through this (6 DOF) can be obtained.

4.3 Data Collection

In our experiment, two rigid bodies are defined i.e., vehicle 1 and vehicle 2. Parrot AR 2.0 drone is used as vehicle 1 which is moving in an anti-clockwise circular path whereas vehicle 2 is stationary as shown in Fig. 4.9. It must be noted that our drone is not equipped with sensors which can measure linear and angular velocities of the drone. So this information is currently not available. It is considered that the drone is rotating on a constant altitude.

The optitrack motive cameras are used to track the trajectory of vehicle 1 and the stationary location of vehicle 2 as shown in Fig. 4.9. The live data from the optitrack cameras is recorded with the help of the motive software. In live modes, all cameras are active and the motive software continuously reconstructs the trajectory of the vehicles through the reflections of the markers detected by the cameras. Once data is recorded, post-processing of data is done in matlab to generate the trajectory of the vehicles and calculate the heading angles as shown in Fig. 4.10. In Fig. 4.11, the heading angles at 9 different locations are shown on the trajectory of vehicle 1.

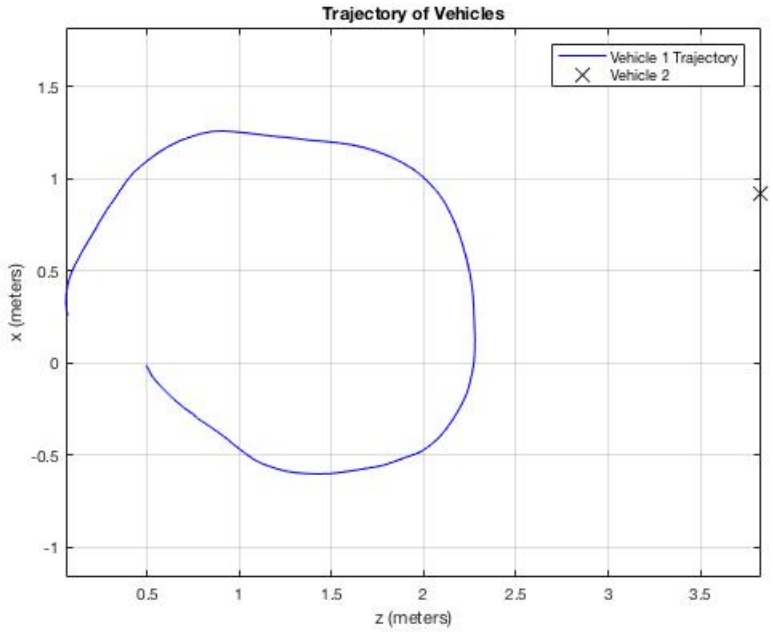

Figure 4.9: Vehicles Trajectory Tracking

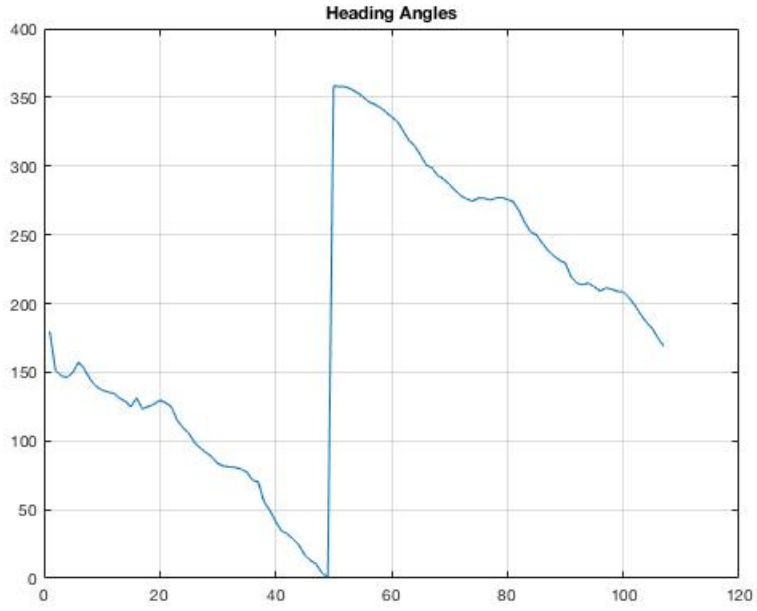

Figure 4.10: Heading Angle Measurement

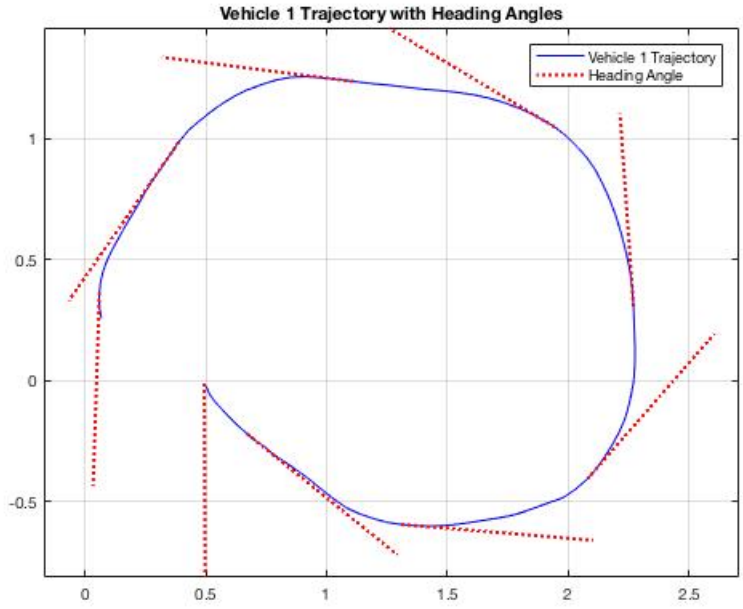

Figure 4.11: Vehicle 1 Trajectory with Heading Angles

Chapter 5

CONCLUSION

5.1 Conclusion and Future work

For the first problem, we analyze observability properties of relative states between two UAS in the presence of constant disturbances. These properties are important for many applications in GPS-denied environments, such as target handoff and relative navigation. We assume that UAS 2 measures UAS 1's position in its own frame. We show that if UAS 1's heading rate is constant and non-zero, the relative states between the two UAS, including the relative heading and the relative disturbance, are locally weakly observable. We further show that when UAS 1 is tracking a stationary ground target under the disturbance, the relative state is also observable. In addition, the range between UAS 1 and the target is observable. We present a simulation example to demonstrate that the relative state can be estimated by an EKF.

For the second problem, we consider relative state estimation between two vehicles with bearing-only measurements. We assume constant angular velocity and linear speed for each vehicle. We examine global observability conditions for four scenarios in which the angular velocity of each vehicle can be zero or non-zero. When the linear speed and angular velocity of vehicle 1 is available to vehicle 2, we establish unobservable conditions when both vehicles are cruising or orbiting. Under these conditions, proper initialization of relative state estimators is required to ensure convergence to the true state. Without vehicle communication, we show that the system is observable if one of the vehicles is orbiting and the other is cruising. When both are orbiting, their angular velocities must be different to ensure observability.

The theoretical analysis provides unobservable conditions that should be avoided in practice for multi-vehicle relative localization. Scenarios close to those unobservable conditions will cause difficulties in accurate and consistent estimation of relative state between vehicles.

Future work includes testing on real flight data, investigating the effect of non-constant disturbances such as wind gusts, and extension to multi-UAS, multi-target scenarios. The future work for our experimental work is to estimate vehicle 1 heading with respect to vehicle 2 using the extended kalman filter to check the accuracy of the algorithm. This work can further be extended to relative heading estimation under disturbances.

Bibliography

[1] Karl J Åström. *Introduction to stochastic control theory*. Courier Corporation, 2012.

[2] A. Awan and H. Bai. Relative heading estimation under constant disturbances. *Accepted by the American Control Conference*, 2017.

[3] He Bai and Randal W Beard. Relative heading estimation for target handoff in GPS-denied environments. In *2016 American Control Conference (ACC)*, pages 336–341. IEEE, 2016.

[4] DP Barnes and JO Gray. Behaviour synthesis for co-operant mobile robot control. In *Control 1991. Control'91., International Conference on*, pages 1135–1140. IET, 1991.

[5] Randal W Beard and Timothy W McLain. *Small Unmanned Aircraft: Theory and Practice*. Princeton University Press, 2012.

[6] James Bruce and Manuela Veloso. Real-time randomized path planning for robot navigation. In *Intelligent Robots and Systems, 2002. IEEE/RSJ International Conference on*, volume 3, pages 2383–2388. IEEE, 2002.

[7] C. I. Byrnes and C. F. Martin. *Global observability and detectability: an overview*, pages 71–89. Springer Berlin Heidelberg, Berlin, Heidelberg, 1988.

[8] Y Uny Cao, Alex S Fukunaga, and Andrew Kahng. Cooperative mobile robotics: Antecedents and directions. *Autonomous robots*, 4(1):7–27, 1997.

[9] NaturalPoint Corporation. Optitrack motion capture system, 2009.

[10] A. Cristofaro and A. Martinelli. 3D cooperative localization and mapping: Observability analysis. In *American Control Conference (ACC), 2011*, pages 1630–1635, June 2011.

[11] Per Enge and Pratap Misra. Special issue on global positioning system. *Proceedings of the IEEE*, 87(1):3–15, 1999.

[12] Jurgen Everaerts et al. The use of unmanned aerial vehicles (uavs) for remote sensing and mapping. *The International Archives of the Photogrammetry, Remote Sensing and Spatial Information Sciences*, 37(2008):1187–1192, 2008.

[13] Paul Fahlstrom and Thomas Gleason. *Introduction to UAV systems*. John Wiley & Sons, 2012.

[14] Adam Fosbury and John Crassidis. Relative navigation of air vehicles. *Journal of Guidance, Control, and Dynamics*, 31(4):824–834, 2008.

[15] Ivan Alexander Getting. Perspective/navigation-the global positioning system. *IEEE spectrum*, 30(12):36–38, 1993.

[16] J. Hardy, J. Strader, J. N. Gross, Y. Gu, M. Keck, J. Douglas, and C. N. Taylor. Unmanned aerial vehicle relative navigation in GPS denied environments. In *2016 IEEE/ION Position, Location and Navigation Symposium (PLANS)*, pages 344–352, April 2016.

[17] Robert Hermann and Arthur J Krener. Nonlinear controllability and observability. *IEEE Transactions on automatic control*, 22(5):728–740, 1977.

[18] Diederich Hinrichsen and Anthony J Pritchard. *Mathematical systems theory I: modelling, state space analysis, stability and robustness*, volume 48. Springer Berlin, 2005.

[19] Vadim Indelman, Pini Gurfil, Ehud Rivlin, and Hector Rotstein. Graph-based distributed cooperative navigation for a general multi-robot measurement model. *The International Journal of Robotics Research*, (9):1057–1080, 2012.

[20] Yoonsoo Kim, Da-Wei Gu, and Ian Postlethwaite. Real-time path planning with limited information for autonomous unmanned air vehicles. *Automatica*, 44(3):696–712, 2008.

[21] Andrea S Laliberte and Albert Rango. Texture and scale in object-based analysis of subdecimeter resolution unmanned aerial vehicle (uav) imagery. *IEEE Transactions on Geoscience and Remote Sensing*, 47(3):761–770, 2009.

[22] A. Martinelli and R. Siegwart. Observability analysis for mobile robot localization. In *IEEE/RSJ International Conference on Intelligent Robots and Systems (IROS)*, pages 1471–1476, Aug 2005.

[23] Luis Merino, Fernando Caballero, J. Ramiro Martínez-de Dios, Iván Maza, and Aníbal Ollero. An unmanned aircraft system for automatic forest fire monitoring and measurement. *Journal of Intelligent & Robotic Systems*, 65(1):533–548, 2012.

[24] Steven Nardone, AG Lindgren, and Kai Gong. Fundamental properties and performance of conventional bearings-only target motion analysis. *IEEE Transactions on automatic control*, 29(9):775–787, 1984.

[25] Steven C Nardone and Vincent J Aidala. Observability criteria for bearings-only target motion analysis. *IEEE Transactions on Aerospace and Electronic Systems*, (2):162–166, 1981.

[26] Albert Rango, Andrea Laliberte, Caiti Steele, Jeffrey E Herrick, Brandon Bestelmeyer, Thomas Schmugge, Abigail Roanhorse, and Vince Jenkins. Using unmanned aerial vehicles for rangelands: current applications and future potentials. *Environmental Practice*, 8(03):159–168, 2006.

[27] Jeffery Saunders and Randal Beard. Tracking a target in wind using a micro air vehicle with a fixed angle camera. In *2008 American Control Conference*, pages 3863–3868. IEEE, 2008.

[28] R. Sharma, R.W. Beard, C.N. Taylor, and S. Quebe. Graph-based observability analysis of bearing-only cooperative localization. *IEEE Transactions on Robotics*, 28(2):522–529, April 2012.

[29] Dan Simon. *Optimal state estimation: Kalman, H infinity, and nonlinear approaches*. John Wiley & Sons, 2006.

[30] Paolo Stegagno, Marco Cognetti, Antonio Franchi, and Giuseppe Oriolo. Mutual localization using anonymous bearing measurements. In *2011 IEEE/RSJ Int. Conf. on Intelligent Robots and Systems*, San Francisco, CA, 2011.

[31] Xiaojun Tang, Jie Yan, and Dudu Zhong. Square-root sigma-point Kalman filtering for spacecraft relative navigation. *Acta Astronautica*, 66(5):704–713, 2010.

[32] Johan Tegin and Jan Wikander. Tactile sensing in intelligent robotic manipulation–a review. *Industrial Robot: An International Journal*, 32(1):64–70, 2005.

[33] Gabriel A Terejanu. Discrete kalman filter tutorial. *University at Buffalo, Department of Computer Science and Engineering, NY*, 14260, 2013.

[34] Lotfi A Zadeh and Charles A Deoser. *Linear system theory*. Robert E. Krieger Publishing Company Huntington, 1976.

[35] Paul Zarchan. *Progress In Astronautics and Aeronautics: Fundamentals of Kalman Filtering: A Practical Approach*, volume 208. Aiaa, 2005.

Appendix A

APPENDIX

A.1 Proof for Proposition 2

Let $d = \tilde{\theta}_3 - \tilde{\theta}_1 \in (-2\pi, 2\pi)$ and rewrite (3.56) as

$$\frac{v_1}{v_2} = \frac{s_{\tilde{\theta}_1 + d} - s_{\tilde{\theta}_1}}{s_d} = c_{\tilde{\theta}_1} - s_{\tilde{\theta}_1} t_{\frac{d}{2}} \tag{A.1}$$

where $t_\cdot = \tan(\cdot)$. First, suppose that $v_1 = v_2$. It follows from (A.1) that either $\tilde{\theta}_1 = 0$ or

$$t_{\frac{d}{2}} + t_{\frac{\tilde{\theta}_1}{2}} = 0, \tag{A.2}$$

which implies

$$d + \tilde{\theta}_1 = \tilde{\theta}_3 = 0. \tag{A.3}$$

If $\tilde{\theta}_1 = 0$, $y_1(t)$ in (3.54) is given by the constant $atan2(b_1, a_1)$, which violates Assumption 1 . Similarly, if $\tilde{\theta}_3 = 0$, $y_3(t)$ is a constant. Therefore, given Assumption 1 and $v_1 = v_2$, no solution of $\tilde{\theta}_3$ to (3.55) and (3.56) exists.

Next, suppose that $v_1 > v_2$, which means that

$$c_{\tilde{\theta}_1} - s_{\tilde{\theta}_1} t_{\frac{d}{2}} > 1. \tag{A.4}$$

Two cases are considered: $s_{\tilde{\theta}_1} > 0$ and $s_{\tilde{\theta}_1} < 0$. The case where $s_{\tilde{\theta}_1} = 0$ is not considered because it does not satisfy (3.55). When $s_{\tilde{\theta}_1} > 0$, i.e., $\tilde{\theta}_1 \in (0, \pi)$, it is further obtained from (A.4)

$$t_{-\frac{d}{2}} > t_{\frac{\tilde{\theta}_1}{2}} > 0. \tag{A.5}$$

Because $\frac{d}{2} \in (-\pi, \pi)$, it follows from (A.5) that

$$\frac{\pi}{2} > -\frac{d}{2} > \frac{\tilde{\theta}_1}{2} > 0 \tag{A.6}$$

or

$$-\frac{\pi}{2} > -\frac{d}{2} > \frac{\tilde{\theta}_1}{2} - \pi > -\pi, \tag{A.7}$$

which implies

$$d + \tilde{\theta}_1 = \tilde{\theta}^3 < 0, \quad 0 > d > -\pi \tag{A.8}$$

or

$$\tilde{\theta}_3 < 2\pi, \quad 2\pi > d > \pi. \tag{A.9}$$

Since $\tilde{\theta}_3 > 0$, (A.8) is impossible. In addition, (A.9) and $\tilde{\theta}_1 \in (0,\pi)$ imply $\tilde{\theta}_3 = \tilde{\theta}_1 + d \in (\pi, 2\pi)$, which means $s_{\tilde{\theta}_3} < 0$. However, (3.55) requires $s_{\tilde{\theta}_3} > 0$ since $s_{\tilde{\theta}_1} > 0$. Thus, if $s_{\tilde{\theta}_1} > 0$, no solution $\tilde{\theta}_3$ exists such that $v_1 > v_2$.

Similarly, if $s_{\tilde{\theta}_1} < 0$, i.e., $\tilde{\theta}_1 \in (\pi, 2\pi)$, so

$$t_{-\frac{d}{2}} < t_{\frac{\tilde{\theta}_1}{2}}, \tag{A.10}$$

which leads to

$$\frac{\pi}{2} < -\frac{d}{2} < \frac{\tilde{\theta}_1}{2} < \pi \tag{A.11}$$

or

$$-\frac{\pi}{2} < -\frac{d}{2} < \frac{\tilde{\theta}_1}{2} - \pi < 0. \tag{A.12}$$

Further simplification results in

$$\tilde{\theta}_3 > 0 \quad \textit{and} \quad -2\pi < d < -\pi, \tag{A.13}$$

or

$$2\pi < \tilde{\theta}_3 \quad \textit{and} \quad 0 < d < \pi. \tag{A.14}$$

Equation (A.13) implies $\tilde{\theta}_1 + d = \tilde{\theta}_3 \in (0,\pi)$. Then $s_{\tilde{\theta}_3} > 0$, which contradicts (3.55) because $s_{\tilde{\theta}_1} < 0$. Equation (A.14) does not hold because $\tilde{\theta}_3 < 2\pi$. Therefore, if $v_1 > v_2$, no solution of $\tilde{\theta}_3$ to (3.55) and (3.56) exists. ■

A.2 Proof for Theorem 1

Proof. Case i). The condition $\frac{v_1}{v_2} > 1$ has been discussed in Section 3.2.1. The case is considered when $v_2 = 0$. The trajectory of vehicle 1 is given by $(p_1^x(0) + v_1 c_{\theta_1} t, p_1^y(0) + v_1 s_{\theta_1} t)$ while vehicle 2 is stationary at $p_2(0)$ with a constant heading $\theta_2(0)$. Then,

$$\tilde{p}_2 = R(\theta_2)^T \begin{pmatrix} p_1^x(0) - p_2^x(0) + v_1 c_{\theta_1} t \\ p_1^y(0) - p_2^y(0) + v_1 s_{\theta_1} t \end{pmatrix}. \tag{A.15}$$

To simplify the derivation, let $\theta_2(0) = 0$. Since the relative heading and position in vehicle 2's frame is to be considered , such a simplification will not affect our result. Thus, $R(\theta_2) = I_2$, $\tilde{\theta} = \theta_1$, and the bearing measurements are given by

$$y(t) = atan2(a_1 + v_1 s_{\theta_1} t, b_1 + v_1 c_{\theta_1} t), \tag{A.16}$$

where $a_1 = p_1^y(0) - p_2^y(0)$ and $b_1 = p_1^y(0) - p_2^y(0)$.

It is now shown that there do not exist a_3, b_3 and θ_3 such that $(a_3, b_3, \theta_3) \neq (a_1, b_1, \theta_1)$, $\theta_i \in [0, 2\pi)$, and

$$\begin{aligned} &atan2(a_1 + v_1 s_{\theta_1} t, b_1 + v_1 c_{\theta_1} t) \\ &= atan2(a_3 + v_1 s_{\theta_3} t, b_3 + v_1 c_{\theta_3} t). \end{aligned} \tag{A.17}$$

Note that (A.17) implies

$$\frac{a_1 + v_1 s_{\theta_1} t}{b_1 + v_1 c_{\theta_1} t} = \frac{a_3 + v_1 s_{\theta_3} t}{b_3 + v_1 c_{\theta_3} t} \tag{A.18}$$

and

$$atan2(a_1, b_1) = atan2(a_3, b_3). \tag{A.19}$$

It is proved by contradiction. Suppose that (A.17)–(A.19) hold with $(a_3, b_3, \theta_3) \neq (a_1, b_1, \theta_1)$. First, two special scenarios are considered. In the first scenario, it is considered that $b_1 + v_1 c_{\theta_1} t \equiv 0$, which implies $\theta_1 = \pm\pi/2$, $b_1 = 0$, and thus $y(t) \equiv \pm\pi/2$. However, Assumption 1 indicates that $y(t)$ is time-varying. Thus, $b_1 + v_1 c_{\theta_1} t$ is not always zero. In the second scenario, it is considered that $\theta_1 = 0$ or π and $a_1 = 0$. Thus, $y(t) \equiv 0$, which contradicts Assumption 1

Then for (A.18) to hold,

$$a_1 b_3 = b_1 a_3 \tag{A.20}$$

$$a_1 c_{\theta_3} + b_3 s_{\theta_1} = a_3 c_{\theta_1} + b_1 s_{\theta_3} \tag{A.21}$$

$$s_{\theta_1} c_{\theta_3} = s_{\theta_3} c_{\theta_1}. \tag{A.22}$$

In addition, since (A.18) holds at $t = 0$, a_i's and b_i's, $i = 1, 3$, must be of the same sign, respectively. Also if $a_1 = 0$, $a_3 = 0$ and if $b_1 = 0$, $b_3 = 0$.

Equation (A.22) implies that $\tan\theta_1 = \tan\theta_3$ or $c_{\theta_1} = c_{\theta_3} = 0$. If $c_{\theta_1} = c_{\theta_3} = 0$, $|s_{\theta_1}| = 1$, $|s_{\theta_3}| = 1$, and (A.21) becomes $b_3 s_{\theta_1} = b_1 s_{\theta_3}$. Because b_1 and b_3 have the same sign, it follows $b_1 = b_3 = 0$ or $\theta_3 = \theta_1$ and $b_1 = b_3 \neq 0$. However, if $b_1 = 0$ and $c_{\theta_1} = 0$, $b_1 + v_1 c_{\theta_1} t = 0$, which has been shown to violate our assumption. Thus, if $c_{\theta_1} = 0$, $\theta_3 = \theta_1$ and $b_1 = b_3 \neq 0$. Then (A.20) implies $a_1 = a_3$.

If $\tan\theta_1 = \tan\theta_3$, $\theta_1 = \theta_3$ or $\theta_1 = \theta_3 \pm \pi$. If $\theta_3 = \theta_1$, it is further obtained from (A.21) that

$$(a_1 - a_3) c_{\theta_1} - (b_1 - b_3) s_{\theta_1} = 0. \tag{A.23}$$

Thus, $(a_1 - a_3, b_1 - b_3)^T$ lies in the null space of $(c_{\theta_1}, -s_{\theta_1})$, which means that $a_1 = a_3 + \ell s_{\theta_1}$ and $b_1 = b_3 + \ell c_{\theta_1}$ for some scalar ℓ. Then (A.20) becomes $(a_3 + \ell s_{\theta_1}) b_3 = (b_3 + \ell c_{\theta_1}) a_3$.

It is now shown that $\ell = 0$ by contradiction. Suppose $\ell \neq 0$. It follows that $s_{\theta_1} b_3 = c_{\theta_1} a_3$. It is shown that if $c_{\theta_1} = 0$, then $a_1 = a_3$ and $b_1 = b_3$, which means that $\ell = 0$. Thus, it is concluded that $c_{\theta_1} \neq 0$. If $b_3 = 0$, $s_{\theta_1} b_3 = c_{\theta_1} a_3$ means $a_3 = 0$, which implies $a_1 = 0$ and $b_1 = 0$ (due to (A.19)). Thus $a_1 = a_3$ and $b_1 = b_3$, which contradicts $\ell \neq 0$. If $b_3 \neq 0$ and $c_{\theta_1} \neq 0$, it follows that $\tan\theta_1 = a_3/b_3$. From (A.20), it is further obtained

$\tan\theta_1 = a_1/b_1$. Therefore, (A.17) equals to a constant a_1/b_1, which contradicts Assumption 1 . Thus, $\ell = 0$, which means that $a_1 = a_3$ and $b_1 = b_3$.

If $\theta_1 = \theta_3 \pm \pi$, (A.21) leads to $(a_1 + a_3)c_{\theta_1} = (b_1 + b_3)s_{\theta_1}$, which together with (A.20) results in $\tan\theta_1 = a_1/b_1 = a_3/b_3$. It then follows from (A.18) that

$$\frac{a_1 + v_1 s_{\theta_1} t}{b_1 + v_1 c_{\theta_1} t} = \frac{a_1}{b_1}, \tag{A.24}$$

which contradicts Assumption 1 . Thus $\theta_1 \neq \theta_3 \pm \pi$.

It is concluded that (a_3, b_3, θ_3) must be the same as (a_1, b_1, θ_1). Since there do not exist a_3, b_3 and θ_3 such that $(a_3, b_3, \theta_3) \neq (a_1, b_1, \theta_1)$ and (A.18) holds, the relative state $(\tilde{p}_2, \tilde{\theta})$ is observable. *Case ii)* In this case, the inertial position $p_i(t)$ of vehicle i, $i = 1, 2$ is obtained, from (**??**) as

$$p_i(t) = d_i + \begin{pmatrix} v_i s_{\omega_i t + \theta_i(0)}/\omega_i \\ -v_i c_{\omega_i t + \theta_i(0)}/\omega_i \end{pmatrix}, \tag{A.25}$$

where $d_i = [d_i^x \; d_i^y]^T \in \mathbb{R}^2$ is a constant vector. Writing $p_1 - p_2$ in vehicle 2's frame,

$$\begin{aligned}
\tilde{p}_2 &= R(\theta_2)^T (p_1 - p_2) \\
&= \begin{pmatrix} c_{\omega_2 t + \theta_2(0)} & s_{\omega_2 t + \theta_2(0)} \\ -s_{\omega_2 t + \theta_2(0)} & c_{\omega_2 t + \theta_2(0)} \end{pmatrix} \left[\begin{pmatrix} d_1^x - d_2^x \\ d_1^y - d_2^y \end{pmatrix} \right. \\
&\quad \left. + \begin{pmatrix} \frac{v_1}{\omega_1} s_{\omega_1 t + \theta_1(0)} - \frac{v_2}{\omega_2} s_{\omega_2 t + \theta_2(0)} \\ -\frac{v_1}{\omega_1} c_{\omega_1 t + \theta_1(0)} + \frac{v_2}{\omega_2} c_{\omega_2 t + \theta_2(0)} \end{pmatrix} \right] \\
&= \begin{pmatrix} c_{\omega_2 t} a + s_{\omega_2 t} b + \frac{v_1}{\omega_1} s_{\tilde{\omega} t + \tilde{\theta}(0)} \\ c_{\omega_2 t} b - s_{\omega_2 t} a - \frac{v_1}{\omega_1} c_{\tilde{\omega} t + \tilde{\theta}(0)} + \frac{v_2}{\omega_2} \end{pmatrix} = \begin{pmatrix} \tilde{p}_2^x(t) \\ \tilde{p}_2^y(t) \end{pmatrix},
\end{aligned} \tag{A.26}$$

where $\tilde{\omega} = \omega_1 - \omega_2$, $\tilde{\theta}(0) = \theta_1(0) - \theta_2(0)$, and a and b are unknown constants dependent on $\theta_2(0)$, $d_1^x - d_2^x$, and $d_1^y - d_2^y$.

There are three unknowns a, b and $\tilde{\theta}(0)$ in $\tilde{p}_2$. Lemma A.1 below proves that given the conditions in *ii)* in Theorem 1 , there exists a unique $(a, b, \tilde{\theta}(0))$ that generate a given set of bearing measurements in (3.53). Therefore, the relative state is observable.

Case iv)

$$\tilde{p}_2 = R(\theta_2(0))^T \left[\begin{pmatrix} d_1^x - d_2^x \\ d_1^y - d_2^y \end{pmatrix} + \begin{pmatrix} \frac{v_1}{\omega_1} s_{\omega_1 t+\theta_1(0)} - v_2 c_{\theta_2(0)} t \\ -\frac{v_1}{\omega_1} c_{\omega_1 t+\theta_1(0)} - v_2 s_{\theta_2(0)} t \end{pmatrix} \right] \tag{A.27}$$

$$= R(\theta_2(0))^T \begin{pmatrix} d_1^x - d_2^x \\ d_1^y - d_2^y \end{pmatrix} + \begin{pmatrix} \frac{v_1}{\tilde{\omega}} s_{\tilde{\omega}t+\tilde{\theta}(0)} - v_2 t \\ -\frac{v_1}{\tilde{\omega}} c_{\tilde{\omega}t+\tilde{\theta}(0)} \end{pmatrix} \tag{A.28}$$

$$= \begin{pmatrix} a + \frac{v_1}{\tilde{\omega}} s_{\tilde{\omega}t+\tilde{\theta}(0)} - v_2 t \\ b - \frac{v_1}{\tilde{\omega}} c_{\tilde{\omega}t+\tilde{\theta}(0)} \end{pmatrix} = \begin{pmatrix} \tilde{p}_2^x(t) \\ \tilde{p}_2^y(t) \end{pmatrix}. \tag{A.29}$$

where a and b are constants related to $\theta_2(0)$, $d_1^x - d_2^x$, and $d_1^y - d_2^y$. It follows from Lemma A.2 below that given measurements $y(t)$ in (3.53), there exists a unique $(a, b, \tilde{\theta}(0))$ that gives rise to $y(t)$. Therefore, the relative state is observable. ■

Lemma A.1 *Suppose $v_1 > 0$, $\omega_1 \neq 0$, $\omega_2 \neq 0$, $\omega_1 \neq \omega_2$, $\omega_2 \neq 2\omega_1$, and $\omega_1 \neq 2\omega_2$. Let $\tilde{\omega} = \omega_1 - \omega_2$. If the constants (a_1, b_1, δ_1) and (a_2, b_2, δ_2) with $\delta_i \in [0, 2\pi)$, $i = 1, 2$, satisfy*

$$\begin{aligned} & atan2\Big(c_{\omega_2 t} b_1 - s_{\omega_2 t} a_1 - \tfrac{v_1}{\omega_1} c_{\tilde{\omega}t+\delta_1} + \tfrac{v_2}{\omega_2}, \\ & c_{\omega_2 t} a_1 + s_{\omega_2 t} b_1 + \tfrac{v_1}{\omega_1} s_{\tilde{\omega}t+\delta_1}\Big) \\ = \quad & atan2\Big(c_{\omega_2 t} b_2 - s_{\omega_2 t} a_2 - \tfrac{v_1}{\omega_1} c_{\tilde{\omega}t+\delta_2} + \tfrac{v_2}{\omega_2}, \\ & c_{\omega_2 t} a_2 + s_{\omega_2 t} b_2 + \tfrac{v_1}{\omega_1} s_{\tilde{\omega}t+\delta_2}\Big), \quad \forall t \geq 0, \end{aligned} \tag{A.30}$$

then $a_1 = a_2$, $b_1 = b_2$, and $\delta_1 = \delta_2$. ■

Proof. First, let $c_{\omega_2 t} b_1 - s_{\omega_2 t} a_1 = A_1 c_{\omega_2 t+\psi_1}$, $c_{\omega_2 t} a_1 + s_{\omega_2 t} b_1 = A_1 s_{\omega_2 t+\psi_1}$, $c_{\omega_2 t} b_2 - s_{\omega_2 t} a_2 = A_2 c_{\omega_2 t+\psi_2}$, and $c_{\omega_2 t} a_2 + s_{\omega_2 t} b_2 = A_2 s_{\omega_2 t+\psi_2}$, where $A_i = \sqrt{a_i^2 + b_i^2}$, $c_{\psi_i} = b_i / A_i$, and $s_{\psi_i} = a_i / A_i$, $i = 1, 2$. Note that $A_i \geq 0$, $i = 1, 2$. When $a_i = b_i = 0$, $A_i = 0$ and ψ_i can be arbitrary.

Note that the left and right sides of (A.30) are the bearing angles generated by the initial conditions (a_1, b_1, δ_1) and (a_2, b_2, δ_2), respectively. Then (A.30) yields

$$\begin{aligned} & (A_1 c_{\omega_2 t+\psi_1} - \tfrac{v_1}{\omega_1} c_{\tilde{\omega}t+\delta_1} + \tfrac{v_2}{\omega_2})(A_2 s_{\omega_2 t+\psi_2} + \tfrac{v_1}{\omega_1} s_{\tilde{\omega}t+\delta_2}) \\ = \quad & (A_1 s_{\omega_2 t+\psi_1} + \tfrac{v_1}{\omega_1} s_{\tilde{\omega}t+\delta_1})(A_2 c_{\omega_2 t+\psi_2} - \tfrac{v_1}{\omega_1} c_{\tilde{\omega}t+\delta_2} + \tfrac{v_2}{\omega_2}). \end{aligned} \tag{A.31}$$

Expanding (A.31),

$$\begin{aligned} & A_1 A_2 s_{\psi_2-\psi_1} - \frac{v_1^2}{\omega_1^2} s_{\delta_2-\delta_1} + \frac{A_1 v_1}{\omega_1} s_{\omega_1 t+\psi_1+\delta_2} - \frac{A_2 v_1}{\omega_1} s_{\omega_1 t+\delta_1+\psi_2} \\ & + \frac{A_2 v_2}{\omega_2} s_{\omega_2 t+\psi_2} - \frac{A_1 v_2}{\omega_2} s_{\omega_2 t+\psi_1} + \frac{v_2 v_1}{\omega_2 \omega_1} s_{\tilde{\omega}t+\delta_2} - \frac{v_2 v_1}{\omega_2 \omega_1} s_{\tilde{\omega}t+\delta_1} = 0. \end{aligned} \tag{A.32}$$

Because $\omega_i \neq 0$, $i = 1, 2$, $\tilde{\omega} \neq -\omega_2$ and $\tilde{\omega} \neq \omega_1$. Because $\omega_1 \neq 2\omega_2$, $\tilde{\omega} \neq \omega_2$. Because $\omega_2 \neq 2\omega_1$, $\tilde{\omega} \neq -\omega_1$. Thus, $\tilde{\omega} \neq \pm\omega_2$, $\tilde{\omega} \neq \pm\omega_1$, and the sinusoidal terms in (A.32) contain three distinct frequencies. Then

for (A.32) to hold,

$$A_1 A_2 s_{\psi_2-\psi_1} = \frac{v_1^2}{\omega_1^2} s_{\delta_2-\delta_1} \tag{A.33}$$

$$\frac{A_1 v_1}{\omega_1} s_{\omega_1 t+\psi_1+\delta_2} = \frac{A_2 v_1}{\omega_1} s_{\omega_1 t+\delta_1+\psi_2} \tag{A.34}$$

$$\frac{A_2 v_2}{\omega_2} s_{\omega_2 t+\psi_2} = \frac{A_1 v_2}{\omega_2} s_{\omega_2 t+\psi_1} \tag{A.35}$$

$$\frac{v_2 v_1}{\omega_2 \omega_1} s_{\bar{\omega} t+\delta_2} = \frac{v_2 v_1}{\omega_2 \omega_1} s_{\bar{\omega} t+\delta_1}. \tag{A.36}$$

It follows from (A.35) that $A_1 = A_2 = 0$ or $A_1 = A_2 \neq 0$ and $\psi_1 = \psi_2$, which both mean that $a_1 = a_2$ and $b_1 = b_2$. Also (A.36) leads to $\delta_2 = \delta_1$. Thus, $(a_1, b_1, \delta_1) = (a_2, b_2, \delta_2)$.

■

Remark 1: When $\omega_1 = \omega_2$, $\omega_2 = 2\omega_1$, or $\omega_1 = 2\omega_2$, the four equations in (A.33)–(A.36) are reduced to three or two equations. For example, if $\omega_1 = \omega_2$, (A.33)–(A.36) become the following two equations:

$$A_1 A_2 s_{\psi_2-\psi_1} + \frac{v_2 v_1}{\omega_1^2} s_{\delta_2} = \frac{v_1^2}{\omega_1^2} s_{\delta_2-\delta_1} + \frac{v_2 v_1}{\omega_1^2} s_{\delta_1} \tag{A.37}$$

$$\frac{A_1 v_1}{\omega_1} s_{\omega_1 t+\psi_1+\delta_2} + \frac{A_2 v_2}{\omega_1} s_{\omega_1 t+\psi_2} = \frac{A_2 v_1}{\omega_1} s_{\omega_1 t+\delta_1+\psi_2} + \frac{A_1 v_2}{\omega_1} s_{\omega_1 t+\psi_1}. \tag{A.38}$$

Besides the trivial solution $(A_2, \psi_2, \delta_2) = (A_1, \psi_1, \delta_1)$, the other two solutions to (A.37) and (A.38) are *a)* $\psi_2 = \psi_1,\ \delta_2 = \delta^*,\ A_2 = -A^*$ and *b)* $\psi_2 = \psi_1 - \pi,\ \delta_2 = \delta^*,\ A_2 = A^*$, where

$$\delta^* = -2\arctan\left(\frac{v_1 - v_2}{(v_1 + v_2)\tan\frac{\delta_1}{2}}\right),\ A^* = A_1 \frac{v_1^2 - v_2^2}{v_1^2 - 2c_{\delta_1} v_1 v_2 + v_2^2}. \tag{A.39}$$

Solution *a)* holds if $v_1 < v_2$ and *b)* holds if $v_1 > v_2$. If $v_1 = v_2$, both solutions become $A_2 = 0$ and $\delta_2 = 0$. Then the right hand side of (A.30) becomes $atan2(0,0)$, which is physically impossible. Thus, the system is observable if $v_1 = v_2$.

If $v_1 > v_2$, a time t^* is picked such that $A_1 s_{\omega_2 t^*+\psi_1} = A_2 s_{\omega_2 t^*+\psi_2} = 0$. Such a t^* exists because $\psi_2 = \psi_1 - \pi$. Then the second argument of the *atan2* function on both sides of (A.30) becomes $\frac{v_1}{\omega_1} s_{\delta_1}$ and $\frac{v_1}{\omega_1} s_{\delta_2}$, respectively. It is also noted from δ^* in (A.39) and $\delta_2 = \delta^*$ that if $\delta_1 \in (0,\pi)$, $\delta_2 \in (\pi, 2\pi)$ and if $\delta_1 \in (\pi, 2\pi)$, $\delta_2 \in (0,\pi)$. Thus, $\frac{v_1}{\omega_1} s_{\delta_1}$ and $\frac{v_1}{\omega_1} s_{\delta_2}$ are of opposite signs, which contradicts (A.30) at time t^*. It follows that the system is observable when $v_1 > v_2$. Unobservable scenarios occur only when $v_1 < v_2$ (see e.g., Fig. 3.7).

When $\omega_1 = 2\omega_2$, (A.33)–(A.36) become

$$A_1 A_2 s_{\psi_2-\psi_1} = \frac{v_1^2}{4\omega_2^2} s_{\delta_2-\delta_1} \tag{A.40}$$

$$\frac{A_1 v_1}{2\omega_2} s_{2\omega_2 t+\delta_2+\psi_1} = \frac{A_2 v_1}{2\omega_2} s_{2\omega_2 t+\delta_1+\psi_2} \tag{A.41}$$

$$A_2 s_{\omega_2 t+\psi_2} + \frac{v_1}{2\omega_2} s_{\omega_2 t+\delta_2} = A_1 s_{\omega_2 t+\psi_1} + \frac{v_1}{2\omega_2} s_{\omega_2 t+\delta_1}. \tag{A.42}$$

From (A.41), $A_1 = A_2$ and $\delta_2 + \psi_1 = \delta_1 + \psi_2$ are obtained, which means that $\delta_2 - \delta_1 = \psi_2 - \psi_1 := \Delta$.

To search for unobservable scenarios, it is assumed that $\Delta \neq 0$. It follows from (A.40) that either $A_1 = \frac{v_1}{2|\omega_2|}$ or $\Delta = \pi$. When $\omega_2 > 0$, (A.42) holds whenever $\psi_1 = \delta_1 + \pi$ for arbitrary Δ. When $\omega_2 < 0$, (A.42) holds whenever $\psi_1 = \delta_1$ for arbitrary Δ.

Therefore, the unobservable scenarios for $\omega_1 = 2\omega_2$ are characterized by the following two initial conditions: i) $A_1 = A_2 = \frac{v_1}{2|\omega_2|}$, $\omega_1 = 2\omega_2$, $\delta_2 - \delta_1 = \psi_2 - \psi_1$, and ii) $\omega_2 > 0$, $\psi_1 = \delta_1 + \pi$, or $\omega_2 < 0$, $\psi_1 = \delta_1$.

A similar analysis can be conducted and the unobservable scenarios can be characterized for $\omega_2 = 2\omega_1$.

■

Lemma A.2 *Suppose $v_1 > 0$ and $\tilde{\omega} \neq 0$. If the constants (a_1, b_1, δ_1) and (a_2, b_2, δ_2), with $\delta_i \in [0, 2\pi)$, $i = 1, 2$, satisfy*

$$\begin{aligned} & atan2(b_1 - \tfrac{v_1}{\tilde{\omega}} c_{\tilde{\omega}t+\delta_1}, a_1 + \tfrac{v_1}{\tilde{\omega}} s_{\tilde{\omega}t+\delta_1} - v_2 t) \\ = \quad & atan2(b_2 - \tfrac{v_1}{\tilde{\omega}} c_{\tilde{\omega}t+\delta_2}, a_2 + \tfrac{v_1}{\tilde{\omega}} s_{\tilde{\omega}t+\delta_2} - v_2 t), \quad \forall t \geq 0, \end{aligned} \tag{A.43}$$

then $a_1 = a_2$, $b_1 = b_2$, and $\delta_1 = \delta_2$. ■

Proof. From (A.43),

$$\begin{aligned} & (b_1 - \tfrac{v_1}{\tilde{\omega}} c_{\tilde{\omega}t+\delta_1})(a_2 + \tfrac{v_1}{\tilde{\omega}} s_{\tilde{\omega}t+\delta_2} - v_2 t) \\ = \quad & (a_1 + \tfrac{v_1}{\tilde{\omega}} s_{\tilde{\omega}t+\delta_1} - v_2 t)(b_2 - \tfrac{v_1}{\tilde{\omega}} c_{\tilde{\omega}t+\delta_2}), \end{aligned} \tag{A.44}$$

which leads to

$$\begin{aligned} & b_1(a_2 + \tfrac{v_1}{\tilde{\omega}} s_{\tilde{\omega}t+\delta_2} - v_2 t) - \tfrac{v_1}{\tilde{\omega}} c_{\tilde{\omega}t+\delta_1}(a_2 + \tfrac{v_1}{\tilde{\omega}} s_{\tilde{\omega}t+\delta_2} - v_2 t) \\ & = b_2(a_1 + \tfrac{v_1}{\tilde{\omega}} s_{\tilde{\omega}t+\delta_1} - v_2 t) - \tfrac{v_1}{\tilde{\omega}} c_{\tilde{\omega}t+\delta_2}(a_1 + \tfrac{v_1}{\tilde{\omega}} s_{\tilde{\omega}t+\delta_1} - v_2 t). \end{aligned} \tag{A.45}$$

Expanding (A.45),

$$\begin{aligned} & b_1 a_2 - b_2 a_1 - \frac{a_2 v_1}{\tilde{\omega}} c_{\tilde{\omega}t+\delta_1} + \frac{b_1 v_1}{\tilde{\omega}} s_{\tilde{\omega}t+\delta_2} + \frac{a_1 v_1}{\tilde{\omega}} c_{\tilde{\omega}t+\delta_2} \\ & - \frac{b_2 v_1}{\tilde{\omega}} s_{\tilde{\omega}t+\delta_1} - b_1 v_2 t + b_2 v_2 t - \frac{v_1^2}{\tilde{\omega}^2} c_{\tilde{\omega}t+\delta_1} s_{\tilde{\omega}t+\delta_2} + \frac{v_1^2}{\tilde{\omega}^2} c_{\tilde{\omega}t+\delta_2} s_{\tilde{\omega}t+\delta_1} \\ & + \frac{v_1 v_2}{\tilde{\omega}} c_{\tilde{\omega}t+\delta_1} t - \frac{v_1 v_2}{\tilde{\omega}} c_{\tilde{\omega}t+\delta_2} t = 0. \end{aligned} \tag{A.46}$$

For (A.46) to hold,

$$b_1 a_2 - b_2 a_1 + \frac{v_1^2}{\tilde{\omega}^2} s_{\delta_1 - \delta_2} = 0 \tag{A.47}$$

$$-\frac{a_2 v_1}{\tilde{\omega}} c_{\tilde{\omega}t+\delta_1} + \frac{b_1 v_1}{\tilde{\omega}} s_{\tilde{\omega}t+\delta_2} = -\frac{a_1 v_1}{\tilde{\omega}} c_{\tilde{\omega}t+\delta_2} + \frac{b_2 v_1}{\tilde{\omega}} s_{\tilde{\omega}t+\delta_1} \tag{A.48}$$

$$b_1 v_2 t = b_2 v_2 t \tag{A.49}$$

$$\frac{v_1}{\tilde{\omega}} c_{\tilde{\omega}t+\delta_1} v_2 t = \frac{v_1}{\tilde{\omega}} c_{\tilde{\omega}t+\delta_2} v_2 t. \tag{A.50}$$

Since v_1 and v_2 are not zero, it is obtained from (A.50) that $\delta_1 = \delta_2$. Equation (A.49) indicates $b_1 = b_2$. Given $\delta_1 = \delta_2$ and $b_1 = b_2$, equation (A.48) is simplified to

$$a_2 c_{\tilde{\omega}t+\delta_1} = a_1 c_{\tilde{\omega}t+\delta_1}, \tag{A.51}$$

which shows $a_1 = a_2$.

■

A.3 Proof for Proposition 3

Following the proof for Lemma A.2, it is proved that if the constants $(a_1, b_1, \delta_1, \alpha_1, \tilde{\omega}_1)$ and $(a_2, b_2, \delta_2, \alpha_2, \tilde{\omega}_2)$, $\delta_i \in [0, 2\pi)$, $\alpha_i > 0$, $\tilde{\omega}_i \neq 0$, $i = 1, 2$, satisfy

$$\begin{aligned} & atan2(b_1 + \tfrac{\alpha_1}{\tilde{\omega}_1} c_{\tilde{\omega}_1 t+\delta_1}, a_1 - \tfrac{\alpha_1}{\tilde{\omega}_1} s_{\tilde{\omega}_1 t+\delta_1} - v_2 t) \\ = \quad & atan2(b_2 + \tfrac{\alpha_2}{\tilde{\omega}_2} c_{\tilde{\omega}_2 t+\delta_2}, a_2 - \tfrac{\alpha_2}{\tilde{\omega}_2} s_{\tilde{\omega}_2 t+\delta_2} - v_2 t), \quad \forall t \geq 0, \end{aligned} \tag{A.52}$$

then $(a_1, b_1, \delta_1, \alpha_1, \tilde{\omega}_1) = (a_2, b_2, \delta_2, \alpha_2, \tilde{\omega}_2)$. Note that $\tilde{\omega}_i$ and α_i, $i = 1, 2$, represent two potential solutions to $\tilde{\omega} = \omega_1 - \omega_2$ and v_1 in (A.43), respectively. Since $\tilde{\omega} \neq 0$, $\tilde{\omega}_i \neq 0$ is required. Since $v_1 > 0$, $\alpha_i > 0$ is required.

It is shown $\tilde{\omega}_1 = \tilde{\omega}_2$ by contradiction. Suppose that $\tilde{\omega}_1 \neq \tilde{\omega}_2$. Similarly to the proof for Lemma A.2, expand (A.52), group alike terms and obtain

$$\begin{aligned} & b_1 a_2 - a_1 b_2 + (b_2 v_2 t - b_1 v_2 t) + (\frac{\alpha_2}{\tilde{\omega}_2} v_2 c_{\tilde{\omega}_2 t+\delta_2} - \frac{\alpha_1}{\tilde{\omega}_1} v_2 c_{\tilde{\omega}_1 t+\delta_1}) t \\ & + \frac{\alpha_1}{\tilde{\omega}_1} \frac{\alpha_2}{\tilde{\omega}_2} s_{(\tilde{\omega}_1 - \tilde{\omega}_2)t+\delta_1-\delta_2} + \frac{\alpha_1}{\tilde{\omega}_1} a_2 c_{\tilde{\omega}_1 t+\delta_1} - \frac{\alpha_2}{\tilde{\omega}_2} a_1 c_{\tilde{\omega}_2 t+\delta_2} \\ & - \frac{\alpha_2}{\tilde{\omega}_2} b_1 s_{\tilde{\omega}_2 t+\delta_2} + \frac{\alpha_1}{\tilde{\omega}_1} b_2 s_{\tilde{\omega}_1 t+\delta_1} = 0. \end{aligned} \tag{A.53}$$

For (A.53) to hold,

$$b_1 v_2 t = b_2 v_2 t \tag{A.54}$$

$$\frac{\alpha_1}{\tilde{\omega}_1} v_2 c_{\tilde{\omega}_1 t+\delta_1} t = \frac{\alpha_2}{\tilde{\omega}_2} v_2 c_{\tilde{\omega}_2 t+\delta_2} t. \tag{A.55}$$

Equation (A.54) holds when $b_1 = b_2$. Equation (A.55) holds in two cases: 1) $\tilde{\omega}_1 = \tilde{\omega}_2$, $\delta_1 = \delta_2$, and $\alpha_1 = \alpha_2$, and 2) $\tilde{\omega}_1 = -\tilde{\omega}_2$, $\delta_1 = -\delta_2 \pm \pi$, and $\alpha_1 = \alpha_2$. Since it is assumed that $\tilde{\omega}_1 \neq \tilde{\omega}_2$, case 1) cannot be true.

It is then shown that case 2) cannot be true either, thereby proving $\tilde{\omega}_1 = \tilde{\omega}_2$. For case 2), substitute $b_1 = b_2$, $\tilde{\omega}_1 = -\tilde{\omega}_2$, $\delta_1 = -\delta_2 \pm \pi$, and $\alpha_1 = \alpha_2$ into (A.53) and note that the frequency of the $\frac{\alpha_1}{\tilde{\omega}_1} \frac{\alpha_2}{\tilde{\omega}_2} s_{(\tilde{\omega}_1 - \tilde{\omega}_2)t+\delta_1-\delta_2}$ term is $2\tilde{\omega}_2$, which is different from the frequencies of all the other terms. Thus, $\frac{\alpha_1}{\tilde{\omega}_1} \frac{\alpha_2}{\tilde{\omega}_2} s_{(\tilde{\omega}_1 - \tilde{\omega}_2)t+\delta_1-\delta_2}$ must be zero, indicating $\alpha_1 = 0$ or $\alpha_2 = 0$. However, it is assumed that $\alpha_i > 0$, $i = 1, 2$. Thus, case 2) is invalid and $\tilde{\omega}_1 = \tilde{\omega}_2$.

Since (A.55) holds only when $\tilde{\omega}_1 = \tilde{\omega}_2$, $\delta_1 = \delta_2$, and $\alpha_1 = \alpha_2$, verify from (A.53) that $a_1 = a_2$.

A.4 Proof for Proposition 4

Similarly to the proof for Lemma A.1, suppose that $(a_1, b_1, \delta_1, \alpha_1, \tilde{\omega}_1)$ and $(a_2, b_2, \delta_2, \alpha_2, \tilde{\omega}_2)$ with $\delta_i \in [0, 2\pi)$, $\alpha_i > 0$, $i = 1, 2$, satisfy

$$\begin{aligned} & atan2\Big(c_{\omega_2 t} b_1 - s_{\omega_2 t} a_1 - \tfrac{\alpha_1}{\bar{\omega}_1} c_{\tilde{\omega}_1 t + \delta_1} + \tfrac{v_2}{\omega_2}\,, \\ & c_{\omega_2 t} a_1 + s_{\omega_2 t} b_1 + \tfrac{\alpha_1}{\bar{\omega}_1} s_{\tilde{\omega}_1 t + \delta_1}\Big) \\ = \quad & atan2\Big(c_{\omega_2 t} b_2 - s_{\omega_2 t} a_2 - \tfrac{\alpha_2}{\bar{\omega}_2} c_{\tilde{\omega}_2 t + \delta_2} + \tfrac{v_2}{\omega_2}\,, \\ & c_{\omega_2 t} a_2 + s_{\omega_2 t} b_2 + \tfrac{\alpha_2}{\bar{\omega}_2} s_{\tilde{\omega}_2 t + \delta_2}\Big), \quad \forall t \geq 0, \end{aligned} \tag{A.56}$$

where $\bar{\omega}_i = \tilde{\omega}_i + \omega_2$, $i = 1, 2$ and α_i and $\tilde{\omega}_i$, $i = 1, 2$, represent two potential solutions to v_1 and $\tilde{\omega} = \omega_1 - \omega_2$ in (A.30), respectively. Similarly, $\bar{\omega}_i$, $i = 1, 2$, correspond to two possible solutions to ω_1 and $\bar{\omega}_i \neq 0$.

Let $c_{\omega_2 t} b_1 - s_{\omega_2 t} a_1 = A_1 c_{\omega_2 t + \psi_1}$, $c_{\omega_2 t} a_1 + s_{\omega_2 t} b_1 = A_1 s_{\omega_2 t + \psi_1}$, $c_{\omega_2 t} b_2 - s_{\omega_2 t} a_2 = A_2 c_{\omega_2 t + \psi_2}$, and $c_{\omega_2 t} a_2 + s_{\omega_2 t} b_2 = A_2 s_{\omega_2 t + \psi_2}$, where $A_i = \sqrt{a_i^2 + b_i^2}$, $c_{\psi_i} = b_i / A_i$, and $s_{\psi_i} = a_i / A_i$, $i = 1, 2$. Note that $A_i \geq 0$, $i = 1, 2$. When $a_i = b_i = 0$, $A_i = 0$ and ψ_i can be arbitrary. Then rewrite (A.56) as

$$\begin{aligned} & (A_1 c_{\omega_2 t + \psi_1} - \tfrac{\alpha_1}{\bar{\omega}_1} c_{\tilde{\omega}_1 t + \delta_1} + \tfrac{v_2}{\omega_2})(A_2 s_{\omega_2 t + \psi_2} + \tfrac{\alpha_2}{\bar{\omega}_2} s_{\tilde{\omega}_2 t + \delta_2}) \\ & = (A_1 s_{\omega_2 t + \psi_1} + \tfrac{\alpha_1}{\bar{\omega}_1} s_{\tilde{\omega}_1 t + \delta_1})(A_2 c_{\omega_2 t + \psi_2} - \tfrac{\alpha_2}{\bar{\omega}_2} c_{\tilde{\omega}_2 t + \delta_2} + \tfrac{v_2}{\omega_2}). \end{aligned} \tag{A.57}$$

Expanding (A.57) yields

$$\begin{aligned} & A_1 A_2 s_{\psi_2 - \psi_1} + \frac{A_1 \alpha_2}{\bar{\omega}_2} c_{\omega_2 t + \psi_1} s_{\tilde{\omega}_2 t + \delta_2} - \frac{A_2 \alpha_1}{\bar{\omega}_1} c_{\tilde{\omega}_1 t + \delta_1} s_{\omega_2 t + \psi_2} \\ & - \frac{\alpha_1 \alpha_2}{\bar{\omega}_1 \bar{\omega}_2} c_{\tilde{\omega}_1 t + \delta_1} s_{\tilde{\omega}_2 t + \delta_2} + \frac{A_2 v_2}{\omega_2} s_{\omega_2 t + \psi_2} + \frac{v_2 \alpha_2}{\omega_2 \bar{\omega}_2} s_{\tilde{\omega}_2 t + \delta_2} \\ & = -\frac{A_1 \alpha_2}{\bar{\omega}_2} s_{\omega_2 t + \psi_1} c_{\tilde{\omega}_2 t + \delta_2} + \frac{A_1 v_2}{\omega_2} s_{\omega_2 t + \psi_1} + \frac{A_2 \alpha_1}{\bar{\omega}_1} s_{\tilde{\omega}_1 t + \delta_1} c_{\omega_2 t + \psi_2} \\ & - \frac{\alpha_1 \alpha_2}{\bar{\omega}_1 \bar{\omega}_2} s_{\tilde{\omega}_1 t + \delta_1} c_{\tilde{\omega}_2 t + \delta_2} + \frac{v_2 \alpha_1}{\omega_2 \bar{\omega}_1} s_{\tilde{\omega}_1 t + \delta_1}, \end{aligned} \tag{A.58}$$

which is simplified to

$$\begin{aligned} & A_1 A_2 s_{\psi_2 - \psi_1} - \frac{\alpha_1 \alpha_2}{\bar{\omega}_1 \bar{\omega}_2} s_{(\tilde{\omega}_2 - \tilde{\omega}_1) t + \delta_2 - \delta_1} + \frac{A_1 \alpha_2}{\bar{\omega}_2} s_{\tilde{\omega}_2 t + \delta_2 + \psi_1} \\ & - \frac{A_2 \alpha_1}{\bar{\omega}_1} s_{\tilde{\omega}_1 t + \psi_2 + \delta_1} - \frac{A_1 v_2}{\omega_2} s_{\omega_2 t + \psi_1} + \frac{A_2 v_2}{\omega_2} s_{\omega_2 t + \psi_2} \\ & + \frac{v_2 \alpha_2}{\omega_2 \bar{\omega}_2} s_{\tilde{\omega}_2 t + \delta_2} - \frac{v_2 \alpha_1}{\omega_2 \bar{\omega}_1} s_{\tilde{\omega}_1 t + \delta_1} = 0. \end{aligned} \tag{A.59}$$

Proof for Part a) To prove that the system is not weakly observable when $\omega_1 = \omega_2$, set $\bar{\omega}_1 = \bar{\omega}_2 = \omega_2$, which means that $\tilde{\omega}_1 = \tilde{\omega}_2 = 0$. Then (A.59) is equivalent to

$$A_1 A_2 s_{\psi_2 - \psi_1} - \frac{\alpha_1 \alpha_2}{\bar{\omega}_1 \bar{\omega}_2} s_{\delta_2 - \delta_1} + \frac{v_2 \alpha_2}{\omega_2 \bar{\omega}_2} s_{\delta_2} - \frac{v_2 \alpha_1}{\omega_2 \bar{\omega}_1} s_{\delta_1} = 0 \tag{A.60}$$

and

$$A_1 \alpha_2 s_{\omega_2 t + \delta_2 + \psi_1} - A_2 \alpha_1 s_{\omega_2 t + \psi_2 + \delta_1} - A_1 v_2 s_{\omega_2 t + \psi_1} + A_2 v_2 s_{\omega_2 t + \psi_2} = 0. \tag{A.61}$$

Given any $(A_1,\psi_1,\delta_1,\alpha_1)$, use (A.60) and (A.61) to solve for $(A_2,\psi_2,\delta_2,\alpha_2)$. Solutions to $(A_2,\psi_2,\delta_2,\alpha_2)$ correspond to unobservable scenarios. Since (A.60) provides one constraint and (A.61) provides two constraints in terms of the magnitude and phase of the sinusoids, there are three independent constraints for four unknown variables $(A_2,\psi_2,\delta_2,\alpha_2)$. The Jacobian matrix of the constraints evaluated at $(A_2,\psi_2,\delta_2,\alpha_2) = (A_1,\psi_1,\delta_1,\alpha_1)$ has a nontrivial null space, which implies that a $(A_2,\psi_2,\delta_2,\alpha_2)$ arbitrarily close to $(A_1,\psi_1,\delta_1,\alpha_1)$ always exists. Thus, the state is not weakly observable.

Proof for Part b) To prove *part b)* of Proposition 4 , first consider the case where $\tilde{\omega}_1 \neq \tilde{\omega}_2$, which means that $\bar{\omega}_1 \neq \bar{\omega}_2$. Given that the system is unobservable when $\omega_1 = \omega_2$, it is also assumed that $\bar{\omega}_1 \neq \omega_2$ in the rest of the proof.

In (A.59), there are six sinusoidal terms

$$T_1 = -\frac{\alpha_1\alpha_2}{\bar{\omega}_1\bar{\omega}_2} s_{(\tilde{\omega}_2-\tilde{\omega}_1)t+\delta_2-\delta_1},\ T_2 = \frac{A_1\alpha_2}{\bar{\omega}_2} s_{\tilde{\omega}_2 t+\delta_2+\psi_1}, \tag{A.62}$$

$$T_3 = -\frac{A_2\alpha_1}{\bar{\omega}_1} s_{\tilde{\omega}_1 t+\psi_2+\delta_1},\ T_4 = -\frac{A_1 v_2}{\omega_2} s_{\omega_2 t+\psi_1} + \frac{A_2 v_2}{\omega_2} s_{\omega_2 t+\psi_2}, \tag{A.63}$$

$$T_5 = \frac{v_2\alpha_2}{\omega_2\bar{\omega}_2} s_{\tilde{\omega}_2 t+\delta_2},\ T_6 = -\frac{v_2\alpha_1}{\omega_2\bar{\omega}_1} s_{\tilde{\omega}_1 t+\delta_1}. \tag{A.64}$$

It follows from (A.59) that $\sum_{i=1}^{6} T_i = 0$ and $A_1 A_2 s_{\psi_2-\psi_1} = 0$. Next,a number of cases are considered to derive the unobservable conditions in *part b)*.

A) Suppose that none of T_i's is of frequency ω_2 except T_4. It then follows that $T_4 = 0$, which means that $A_1 = A_2 \neq 0$ and $\psi_1 = \psi_2$ or $A_1 = A_2 = 0$.

A1) If $A_1 = A_2 = 0$, $T_2 = T_3 = 0$. Then $\sum_{i=1}^{6} T_i = 0$ leads to $T_1 + T_5 + T_6 = 0$. Note that the magnitudes of T_1, T_5 and T_6 are non-zero, which implies from $T_1 + T_5 + T_6 = 0$ that the frequencies of T_1, T_5 and T_6 must be the same, that is $|\tilde{\omega}_2 - \tilde{\omega}_1| = |\tilde{\omega}_2| = |\tilde{\omega}_1|$. Since $\tilde{\omega}_1 \neq \tilde{\omega}_2$, so $\tilde{\omega}_2 = -\tilde{\omega}_1$. Then $|\tilde{\omega}_2 - \tilde{\omega}_1| = |\tilde{\omega}_1|$ leads to $\tilde{\omega}_1 = 0$ and thus $\bar{\omega}_1 = \omega_2$, which contradicts our assumption. Thus case *A1)* is invalid.

A2) When $A_1 = A_2 \neq 0$ and $\psi_1 = \psi_2$, $\sum_{i=1}^{6} T_i = 0$ leads to $T_1 + T_2 + T_3 + T_5 + T_6 = 0$. Since all the five sinusoids have non-zero magnitudes, either all of them have the same frequency or three of them have one frequency and the other two have another frequency. If all the five sinusoids have the same frequency, the frequencies of T_1, T_5 and T_6 must be the same, which implies $\bar{\omega}_1 = \omega_2$ from case $A1$) and contradicts our assumption. Thus, conditions under which three out of the five sinusoids are of one frequency and the other two sinusoids are of another frequency are searched.

Matlab is used to conduct an extensive search and solve for $\bar{\omega}_1$ and $\bar{\omega}_2$ using the Symbolic toolbox and the "solve" command. The following two conditions are obtained

a1) $\bar{\omega}_1 = \omega_2/3,\ \bar{\omega}_2 = 2\omega_2/3$ or

a2) $\bar{\omega}_1 = 2\omega_2/3,\ \bar{\omega}_1 = \omega_2/3$.

Given *a1)*, T_1, T_3 and T_5 have the same frequency and T_2 and T_6 have a different frequency. Similarly, given *a2)*, T_1, T_2 and T_6 have the same frequency and T_3 and T_5 have a different frequency.

Take *a1)* as an example to illustrate the unobservable conditions. It follows from $\sum_{i=1}^{6} T_i = 0$ and *a1)* that $T_1 + T_3 + T_5 = 0$ and $T_2 + T_6 = 0$. Then the system is not observable for specific conditions of $(A_1, \psi_1, \delta_1, \alpha_1, \delta_2, \alpha_2)$ such that $T_1 + T_3 + T_5 = 0$ and $T_2 + T_6 = 0$ are true and $\alpha_1 \neq \alpha_2$ or $\delta_1 \neq \delta_2$.

B) Suppose that there exists at least one term from T_i, $i = 1, \cdots, 6$, $i \neq 4$, that has frequency ω_2.

B1) Suppose that $A_1 \neq 0$ and $A_2 \neq 0$. In this case, since T_i's all have non-zero magnitudes, $\sum_{i=1}^{6} T_i = 0$ can be satisfied in one of the following scenarios:

1) group the six terms into three groups, each containing two terms. The two terms within each group are of the same frequency;

2) group the six terms into two groups, one group containing four terms and the other containing two terms. The terms within each group are of the same frequency;

3) group the six terms into two groups, one group containing three terms and the other containing three terms. The terms within each group are of the same frequency.

Matlab is used to conduct an extensive search and solve for $\bar{\omega}_1$ and $\bar{\omega}_2$ for each scenario above. The solutions to $\bar{\omega}_1$ are found to be either 0 or ω_2, which contradicts our assumption. Thus, *B1)* is invalid.

B2) Suppose that $A_1 = 0$ and $A_2 \neq 0$. In this case, $T_1 + T_3 + T_4 + T_5 + T_6 = 0$ can be satisfied in the following scenario: group the five terms into two groups, one group containing three terms and the other containing two terms and the terms within each group are of the same frequency. Using Matlab, two conditions are found that achieve this scenario:

b1) $\bar{\omega}_1 = \omega_2/2$, $\bar{\omega}_2 = 3\omega_2/2$ or

b2) $\bar{\omega}_1 = 2\omega_2$, $\bar{\omega}_2 = 3\omega_2$.

In either *b1)* or *b2)*, setting the sum of the sinusoids in each group to zero provides two constraints, resulting in 4 constraints in total. The system is not observable for initial conditions under which those four constraints are satisfied.

B3) $A_1 \neq 0$ and $A_2 = 0$. This is similar to *B2)*. The conditions obtained from Matlab are

b3) $\bar{\omega}_1 = 3\omega_2/2$, $\bar{\omega}_2 = \omega_2/2$ or

b4) $\bar{\omega}_1 = 3\omega_2$, $\bar{\omega}_2 = 2\omega_2$.

B4) $A_1 = A_2 = 0$. This has been considered in *A1)*.

In summary, when $\bar{\omega}_1$ satisfies *a1)* or *a2)* or one of *b1)–b4)*, the system is not observable for specific initial conditions.

Proof for the observability result Based on the proof for *part b)*, it is concluded that when $\bar{\omega}_1$ does not satisfy *a1)* and *a2)* and *b1)–b4)*, $\tilde{\omega}_1 \neq \tilde{\omega}_2$ cannot be true for (A.59) to hold. Thus, it is considered the case

$\tilde{\omega}_1 = \tilde{\omega}_2$, which means that $\bar{\omega}_1 = \bar{\omega}_2$. Because $\bar{\omega}_1$ does not satisfy *b2)* and $\bar{\omega}_1 \neq 0$, so $|\tilde{\omega}_1| \neq |\omega_2|$.

When $\bar{\omega}_1 \neq -\omega_2$, alike terms in (A.59) are equated and obtain

$$A_1 A_2 s_{\psi_2 - \psi_1} = \frac{\alpha_1 \alpha_2}{\bar{\omega}_1 \bar{\omega}_2} s_{\delta_2 - \delta_1} \tag{A.65}$$

$$\frac{A_1 \alpha_2}{\bar{\omega}_1} s_{\bar{\omega}_1 t + \delta_2 + \psi_1} = \frac{A_2 \alpha_1}{\bar{\omega}_1} s_{\bar{\omega}_1 t + \psi_2 + \delta_1} \tag{A.66}$$

$$-\frac{A_1 v_2}{\omega_2} s_{\omega_2 t + \psi_1} = -\frac{A_2 v_2}{\omega_2} s_{\omega_2 t + \psi_2} \tag{A.67}$$

$$\frac{v_2 \alpha_2}{\omega_2 \bar{\omega}_1} s_{\bar{\omega}_1 t + \delta_2} = \frac{v_2 \alpha_1}{\omega_2 \bar{\omega}_1} s_{\bar{\omega}_1 t + \delta_1}. \tag{A.68}$$

From (A.67), $A_1 = A_2 \neq 0$ and $\psi_1 = \psi_2$ or $A_1 = A_2 = 0$, which both imply $a_1 = a_2$ and $b_1 = b_2$. Equation (A.68) leads to $\alpha_1 = \alpha_2$ and $\delta_1 = \delta_2$. Since $\bar{\omega}_1 = \bar{\omega}_2$, it follows that the system is observable.

Proof for Part c) If $\bar{\omega}_1 = \bar{\omega}_2 = -\omega_2$, (A.66) and (A.67) have the same frequency. From (A.59), (A.66) and (A.67) are combined as

$$\begin{aligned} & A_1 \left(\frac{\alpha_1}{\bar{\omega}_1} s_{\bar{\omega}_1 t + \delta_1 + \psi_1} + \frac{v_2}{\bar{\omega}_1} s_{-\bar{\omega}_1 t + \psi_1} \right) \\ = & A_2 \left(\frac{\alpha_1}{\bar{\omega}_1} s_{\bar{\omega}_1 t + \psi_2 + \delta_1} + \frac{v_2}{\bar{\omega}_1} s_{-\bar{\omega}_1 t + \psi_2} \right), \end{aligned} \tag{A.69}$$

where $\alpha_1 = \alpha_2$ and $\delta_1 = \delta_2$ are used from (A.68).

Substituting $\delta_1 = \delta_2$ into (A.65) yields

$$A_1 A_2 s_{\psi_2 - \psi_1} = 0, \tag{A.70}$$

which is satisfied under one of the following conditions:

c1) $\psi_2 = \psi_1$, $A_i \neq 0$;

c2) $\psi_2 = \psi_1 \pm \pi$, $A_i \neq 0$;

c3) $A_1 = 0$ or $A_2 = 0$.

Substituting *c1)* into (A.69) results in $A_1 = A_2$, which means that the system is observable. Substituting *c2)* into (A.69) yields

$$\begin{aligned} & A_1 \left(\frac{\alpha_1}{\bar{\omega}_1} s_{\bar{\omega}_1 t + \delta_1 + \psi_1} + \frac{v_2}{\bar{\omega}_1} s_{-\bar{\omega}_1 t + \psi_1} \right) \\ = & -A_2 \left(\frac{\alpha_1}{\bar{\omega}_1} s_{\bar{\omega}_1 t + \psi_1 + \delta_1} + \frac{v_2}{\bar{\omega}_1} s_{-\bar{\omega}_1 t + \psi_1} \right), \end{aligned} \tag{A.71}$$

which indicates $A_1 = -A_2$. Since $A_1 \geq 0$ and $A_2 \geq 0$, it follows that $A_1 = A_2 = 0$. In this case, ψ_i's are arbitrary because $a_1 = a_2 = b_1 = b_2 = 0$. The system is also observable.

Given *c3)*, if $A_1 = 0$ and $A_2 \neq 0$, (A.69) is reduced to

$$\frac{\alpha_1}{\bar{\omega}_1} s_{\bar{\omega}_1 t + \psi_2 + \delta_1} = \frac{v_2}{\bar{\omega}_1} s_{\bar{\omega}_1 t - \psi_2} \tag{A.72}$$

which leads to $\alpha_1 = \alpha_2 = v_2$ and $\psi_2 = -\delta_1/2$. If $A_1 \neq 0$ and $A_2 = 0$, $\alpha_1 = \alpha_2 = v_2$ and $\psi_1 = -\delta_1/2$ are obtained. Thus, if $v_1 \neq v_2$, (A.72) cannot be true and the system is observable.

If $v_1 = v_2$, the unobservable scenarios are given by the following two conditions i) $\bar{\omega}_1 = \bar{\omega}_2 = -\omega_2$, $\alpha_1 = \alpha_2 = v_2$, and ii) $A_1 = 0$, $A_2 \neq 0$, $\delta_1 = \delta_2 = -2\psi_2$, or $A_1 \neq 0$, $A_2 = 0$, $\delta_1 = \delta_2 = -2\psi_1$, which proves *part c)* in Proposition 4 . ■

VITA

Asad N. Awan

Candidate for the Degree of

Master of Science

Thesis: OBSERVABILITY PROPERTIES OF RELATIVE STATE ESTIMATION BETWEEN TWO VEHICLES IN A GPS-DENIED ENVIRONMENT

Major Field: Electrical Engineering with specialization in Robotics and Controls

Biographical:

Education: Masters of Science in Electrical Engineering at Oklahoma State University, May 2017.
Bachelor of Science in Electrical Engineering at University of Engineering and Technology, Pakistan, August 2011.

Experience: Instrumentation and Controls Engineer at Engro Fertilizers Manufacturing Site, Pakistan, August 2011 - August 2015.

Publications: Asad Awan and He Bai. Relative heading estimation under constant disturbances. Accepted by the American Control Conference, 2017.
He Bai and Asad Awan. Observability properties of relative state estimation in Bearing-Only scenario. Submitted to IEEE Conference on Decision and Control, 2017.